Ecological and evolutionary patterns of virus-host interactions throughout a grassland soil depth profile

George Muscatt[1†], Ryan Cook[2], Andrew Millard[3], Gary D. Bending[1], Eleanor Jameson[1,4]

[1] School of Life Sciences, University of Warwick, Coventry, United Kingdom.

[2] School of Veterinary Medicine and Science, University of Nottingham, Loughborough, United Kingdom.

[3] Department of Genetics and Genome Biology, University of Leicester, Leicester, United Kingdom.

[4] School of Natural Sciences, Bangor University, Bangor, Gwynedd, United Kingdom.

[†] Corresponding author: george.s.muscatt@warwick.ac.uk

Running title: Ecological and evolutionary patterns of viruses throughout a soil depth profile

Abstract

Background: Soil microbes play pivotal roles in global carbon cycling, however the fundamental interactions between microbes and their infecting viruses remain unclear. This is exacerbated with soil depth, where the patterns of viral dispersal, ecology, and evolution are markedly underexplored. To investigate viral communities across soil depth, we leveraged a publicly available metagenomic data set sampled from grassland soil in northern California.

Results: 10,196 non-redundant vOTUs were recovered from soil sampled from 20 cm to 120 cm below the surface. Viral prevalence was high throughout the soil depth profile, with viruses infecting dominant soil phyla, including *Actinomycetota*. Contrary to leading hypotheses, lysogeny did not dominate in the soil viral communities. Viral diversity was investigated at both the population-level (i.e., macro diversity) and strain-level (i.e., micro diversity) to reveal diverse ecological and evolutionary patterns of virus-host interactions in surface and subsurface soil.

Conclusions: By investigating viral micro diversity in soil for the first time, we have uncovered patterns of antagonistic co-evolution across both surface and subsurface soils. Furthermore, we have provided evidence of soil viruses augmenting the remineralisation of soil carbon. While we continue to yield a more comprehensive understanding of soil viral ecology, our work appeals to future researchers to continue to investigate subsurface viral communities.

Key words: Antagonistic co-evolution, Lysogeny, Macro diversity, Micro diversity, Positive selection, Soil depth, Virus-host interactions.

Background

Soil microbes are integral members of terrestrial ecosystems, with microbial metabolism contributing to global carbon cycling [1]. As obligate parasites of microbes, viruses can control their hosts' population size through lytic infections and influence their hosts' metabolic potential through the expression of auxiliary metabolic genes (AMGs) [2–6]. In the oceans, where virus-host interactions have been more thoroughly studied, viral lysis is estimated to turnover ~ 20% of microbial biomass each day [7]. The subsequent liberation of dissolved carbon and nutrients increases microbial respiration and limits trophic transfer up the food web [8, 9]. Despite an appreciation for the ecological roles of viruses in marine ecosystems, the relevant functions of viruses in terrestrial ecosystems have received less attention. To resolve this, recent methodological developments have provided the means to investigate soil viral ecology through metagenomics [10–12], and we are beginning to uncover the ecosystem-level impacts of soil viruses [13].

Integral to understanding soil viral ecology are the fundamentals of viral dispersal, prevalence, and persistence. The consequence of these factors is demonstrated by the structuring of viral communities across gradients of space [14–18], time [13, 16, 17], and root/soil compartment [13, 19]. However, most ecological studies have focussed on surface soils, rendering subsurface viral communities markedly underexplored. This is particularly alarming given the disparity in soil biogeochemistry between surface and subsurface niches. For example, more than half of terrestrial carbon stocks are sequestered in subsurface soils [20], with microbial respiration and biomass turnover dictating long-term carbon storage [21, 22]. Additionally, subsurface microbial communities are key drivers of pollutant biodegradation, thus controlling their fate and dispersal to groundwater resources [23]. Given the pressures of viral infection on the mortality and metabolism of host populations,

66 investigations into subsurface soil ecology could inform global actions for mitigating climate
67 change and promoting bioremediation.

68 Numerous physicochemical properties of soil vary throughout its vertical profile [24, 25].
69 These factors shape the distribution of microbial populations such that community variation
70 with depth is comparable to the variation observed between surface soils from different biomes
71 [26]. Thus, the structuring of microbial communities may reflect variation in microbial
72 responses to nutrient availability between ecological niches. Given the requirement of host
73 cellular machinery for replication and the specificity of host infection, the structuring of viral
74 communities is likely highly dependent on that of their host community. Subsequently, there
75 is great importance in characterising the diversity of fundamental virus-host interactions.

76 Amid exponentially decreasing host biomass, activity, and diversity in subsurface soil [26,
77 27], virus-host interactions are likely to vary considerably with depth. For example,
78 microscopic investigations have found that virus-to-bacteria ratios decrease with soil depth
79 [28]. Lower virus-to-bacteria ratios have been associated with an increased prevalence of
80 lysogeny [28, 29], a latent replication strategy where the viral genome replicates passively
81 within the host's chromosome until induced. Lysogenic infections can have significant impacts
82 on the ecology and evolution of their host communities (hereafter referred to as "eco-
83 evolutionary interactions") [30]. While temperate viruses, capable of lysogeny, have been
84 predicted to dominate in soils [31–33], relevant metagenomic studies have failed to corroborate
85 this [12, 13, 34]. The argument for such increased lysogeny, namely the reduced access to
86 viable hosts [28, 29, 35], has a stronger case in subsurface soil. Therefore, more studies
87 investigating subsurface viruses are required to determine infection strategy preferences
88 throughout the soil depth profile.

89 The co-evolution of viruses and their hosts contributes to the emergence and maintenance
90 of phenotypic diversity in both partners [36–38]. This relationship is inherently antagonistic

since the adaptation of one partner disadvantages the survival of the other. However, we understand very little about in situ antagonistic co-evolution, and even less across environmental gradients such as soil depth. Given the stark differences in nutrient availability over short vertical distances [24, 25], which have been evidenced to impact co-evolution dynamics [39], we hypothesise that the eco-evolutionary interactions between viruses and their hosts vary throughout the soil depth profile. This is likely to implicate soil viruses in the major biogeochemical processes existing throughout soil, as has been demonstrated for marine ecosystems [8, 40].

In this study, we leveraged a publicly available metagenomic data set assembled from Californian grassland soil [41] to investigate viral communities from 20 cm to 115 cm below the soil surface. Grasslands cover ~ 40% of non-glacial land area [42], store a third of global terrestrial carbon [43], and provide numerous ecosystem services from food production to erosion regulation [44]. This presents grassland ecosystems as an ideal model system for investigating the eco-evolutionary interactions between soil viruses and their microbial hosts. Two soil depth profiles were sampled, representing contrasting aboveground vegetation: under a Garry oak tree ("Garry Oak" samples) versus neighbouring grassland ("Hilly grassland" samples). To uncover patterns of viral dispersal, ecology, and evolution across soil depth, we assessed viral diversity at both the population-level (i.e., macro diversity) and strain-level (i.e., micro diversity). This study aimed to answer the following questions: (1) To what extent does soil depth shape the assembly of viral communities, and is this effect consistent between sites? (2) Does lysogeny vary throughout the soil depth profile, such that temperate viruses dominate in subsurface soil? (3) How do the eco-evolutionary interactions between viruses and their hosts vary throughout the soil depth profile?

Methods

Field site.

Soil was sampled previously [41] at the Sagehorn study site within the Eel River Critical Zone Observatory in Northern California. The site is underlain by the Central Belt of the Franciscan Formation, a mélange of sheared argillaceous matrix containing blocks of sandstone and other lithologies [45]. The soil profile comprises a surface organic-rich horizon (~ 30 cm) underlain by a clay-rich horizon (10 cm – 20 cm), directly above saprolite [46]. As a result of the low-porosity bedrock, the critical zone layers become entirely saturated during the winter wet season [46]. Sagehorn is primarily a grassland ecosystem, with scattered Garry oak (*Quercus garryana*) trees. The region has a Mediterranean climate, described by hot, dry summers (from May – September) and cool, wet winters. The average rainfall for the region is ~ 1800 mm, with 1976 mm of precipitation recorded during the year that soil samples were taken [46].

Sample collection.

The collection of soil samples was previously performed at the Sagehorn study site in Northern California in June 2016, by Sharrar et al. [41]. The vertical soil depth profile was sampled at 20 cm, 40 cm, 60 cm, 80 cm, 100 cm, and 115 cm. Soil pits were dug using a jackhammer, and the walls of the pits were sampled on both sides with a sterile scoop, resulting in two samples per soil depth collected approximately 10 cm apart laterally. Soil was sampled at two sites: under a Garry oak tree ("Garry oak" samples) and from the grassland approximately 10 m away ("Hilly grassland" samples), for a total of 24 samples.

Metagenomic data set access.

The metagenomes assembled from each soil sample described above were accessed from NCBI under project accession PRJNA577476 (sample accessions SAMN13153360-SAMN13153383).

Recovery of viral populations.

Viral contigs were predicted from the pooled assembled metagenomes (PRJNA577476). Double-stranded DNA (dsDNA) and single-stranded DNA (ssDNA) viral contigs ≥ 5 kilobase pairs (kb) were predicted with DeepVirFinder v1.0 [47], VIBRANT v1.2.1 [48] and VirSorter v2.2.3 [49], using permissive viral score thresholds where relevant (≥ 0.8 for DeepVirFinder and ≥ 0.5 for VirSorter). The quality of viral contigs predicted from all three tools was assessed with CheckV v0.8.1 [50], and resulting trimmed viral sequences were annotated with DRAM v1.3 [51]. Annotated viral sequences were manually curated following the selection criteria outlined by Guo et al. [52]. Additionally, viral sequences with the most confident prediction scores from DeepVirFinder (with corresponding viral scores ≥ 0.95, $p \leq 0.05$, and length ≥ 10 kb) and from VIBRANT (with corresponding quality scores of "high quality draft" or "complete circular", and length ≥ 10 kb) were retained. Viral sequences were clustered into viral operational taxonomic units (vOTUs) at 95% nucleotide identity across 85% of shorter sequence [53] using anicalc.py and aniclust.py scripts [50], resulting in 10,196 vOTUs ≥ 5 kb, representing approximately species-level viral populations. Additional functional gene annotations were provided with Prokka v1.14.6 [54] using the Prokaryotic Virus Remote Homologous Groups (PHROGs) database [55].

To determine whether any recovered vOTUs represented previously isolated phage species, we clustered our vOTUs with the INfrastructure for a PHAge REference Database (INPHARED) of phage genomes (accessed February 2022) [56] using anicalc.py and

aniclust.py scripts [50]. Viral sequences were considered to represent the same species when they shared 95% nucleotide identity across 85% of shorter sequence [53].

Taxonomy of viral populations.

Taxonomic assessment of vOTUs was achieved through shared protein clustering using vConTACT2 v0.9.22 [57] with the INPHARED phage genome database (accessed February 2022) [56], and otherwise default settings. The resultant genome network was visualised in R v4.0.5 [58] using ggnet2 from GGally v2.1.2 [59] and the Fruchterman-Reingold force-directed algorithm. Nodes (representing viral genomes) were connected by edges (representing shared protein homology), with significant connections forming viral clusters (VCs) representing roughly genus-level groups. Viral genomes sharing overlap with genomes from multiple VCs were considered as singletons. To further interrogate the similarity of recovered vOTUs to a database of $>$ 600,000 environmental phage sequences, we leveraged the web-based PhageClouds tool [60], using an intergenomic distance threshold of 0.21.

The phylogeny of jumbo phage vOTU and "jumbo-related" vOTU genomes was investigated using the DNA polymerase gene. The translated DNA polymerase gene sequences were queried against the INPHARED phage genomes database [56] (accessed June 2022) to identify closely related phage genomes using the ublast command from USEARCH v10.0.240 [61] and a similarity E-value threshold $<$ 0.001. For downstream visualisation, an outgroup of human alphaherpesvirus 1 was included in the analysis. The translated sequences of the DNA polymerase gene from the vOTUs and reference genomes were then aligned using MAFFT v7.271 [62, 63], with automated settings. Phylogenetic trees were constructed using IQ-TREE v1.6.3 [64–66], the Whelan and Goldman protein substitution model, and 1000 bootstrap replicates. Trees were subsequently visualised in R using ggtree v2.5.3 [67–69].

Characterisation of viral populations.

vOTUs were classified as temperate when they were identified by any of the three following methods. Firstly, if the viral contig was excised from a flanking host scaffold by CheckV. Secondly, vOTUs carrying at least one gene associated with lysogeny (i.e., transposase, integrase, excisionase, resolvase, and recombinase) were considered temperate. Lysogeny associated genes were identified using the Pfam domains: PF07508, PF00589, PF01609, PF03184, PF02914, PF01797, PF04986, PF00665, PF07825, PF00239, PF13009, PF16795, PF01526, PF03400, PF01610, PF03050, PF04693, PF07592, PF12762, PF13359, PF13586, PF13610, PF13612, PF13701, PF13737, PF13751, PF13808, PF13843 and PF13358, as previously described [70, 71]. Thirdly, vOTUs which formed a VC with at least one known temperate phage were also considered temperate.

Host assignment was achieved using a combination of methods. Firstly, hosts were inferred using the microbial taxonomy assigned to the scaffold from which proviral sequences were excised from. Secondly, CRISPR spacers identified from assembled scaffolds using PILER-CR v1.06 [72] were used to identify complementary protospacers among vOTU genomes using BLASTn, with default settings and allowing for ≤ 2 mismatches. Additionally, CrisprOpenDB [73] was used with default settings. Lastly, host genera were predicted *de novo* using WIsH v1.0 [74] and a null model trained against 9620 bacterial genomes, as previously described [70]. Given that some vOTUs had conflicting host predictions between methods, and that only a single host was considered per vOTU in our analyses, preferential assignment of hosts was ordered: provirus hosts $>$ CRISPR spacer linkage to MAG $>$ CRISPR spacer linkage to database genome $>$ WIsH *de novo* prediction.

Putative viral-encoded AMGs were identified using DRAM-v [51]. Due to the expected increased false positive signal arising from the high non-viral sequence space in the soil metagenomes, strict curation of candidate AMGs was performed, as suggested [75]. Briefly,

this included genes on viral contigs ≥ 10 kb or complete genomes, with an auxiliary score of 1 – 3, and with both the "M" flag (corresponding to metabolic function) and the "F" flag (corresponding to genes within 5000 bases of the end of the viral contig).

AMGs encoding carbohydrate-active enzymes (CAZymes) were further interrogated for the detection of conserved functional domains using the Conserved Domain Search (CD-Search) service [76, 77]. No CAZymes had the "A" flag from DRAM-v, which indicates tail-association, implicating putative CAZymes with host metabolism instead of viral attachment.

Abundance of viral populations.

vOTU abundance was estimated by mapping raw metagenome reads against vOTU genomes using BBMap [78] with a minimum alignment identity of 90%. vOTUs were only considered present in a sample if ≥ 75% of the contig length was covered ≥ 1× by reads, as recommended [53, 79]. Raw reads were normalised by vOTU genome length and library sequencing depth to generate counts per kilobase million (CPM) using the following formula: ((raw reads / genome length) / sample read depth) × 1 e^6.

Recovery of microbial populations.

Microbial operational taxonomic units (OTUs) were recovered using bacterial and archaeal ribosomal protein S3 (rpS3) sequences, as previously described [41]. Briefly, rpS3 sequences were identified by searching proteins predicted from the assembled metagenomes using a custom hidden Markov model. rpS3 protein taxonomy was subsequently inferred using BLASTp to search against a database of rpS3 proteins [80] with an E-value threshold of 1 e^{-10}. While the vast majority of OTUs were assigned to bacterial phyla, some OTUs were assigned to the archaeal phylum *Euryarchaeota* or unknown phyla (Table S2).

In addition to OTUs, previously reconstructed [41] bacterial and archaeal metagenome-assembled genome (MAG) sequences were accessed. Similarly, most of these genomes belonged to bacterial phyla (Table S3).

Abundance of microbial populations and metagenome-assembled genomes.

The abundance of OTUs and MAGs were estimated by mapping raw metagenome reads against rpS3-containing scaffolds and MAG genomes, respectively, using BBMap with a minimum alignment identity of 98%. OTUs and MAGs were only considered present in a sample if $\geq$ 75% of the contig length was covered. Coverage per base pair was normalised for sample sequencing depth using the following formula: (raw coverage/sample read depth) $\times$ average read depth across samples.

Viral micro diversity.

The nucleotide diversity (π) of viral populations and the proportion of non-synonymous to synonymous polymorphism ratio (pN/pS) of each viral gene in each sample was estimated with Metapop [81] using BAM files from read mapping (see above) and default parameters, including thresholds of $>$ 70% genome coverage and $>$ 10 $\times$ average read depth. The total micro diversity of each sample was calculated by averaging over bootstrapped π values, as previously described [82].

Genes under positive selection were identified with pN/pS ratios $<$ 1. Genes encoding putative ABC transporters were further interrogated for the detection of conserved functional domains using CD-Search.

Consensus vOTU sequences were constructed using the most common allele from variant sites identified using inStrain v1.5.7 [83] and BAM files from read mapping. Variants were called if a site had a minimum of five viral scaffold reads. Strain-level heterogeneity was subsequently estimated by computing the pairwise ANI of these sample-specific consensus

sequences. Pairwise comparisons were only considered for analysis when the genome coverage between samples was > 25%.

Identification of anti-phage systems.

Anti-phage systems were identified from MAGs using DefenseFinder [84, 85] (accessed May 2022), with default settings. Only MAGs carrying complete anti-phage systems i.e., with all genes relating to the anti-phage system detected on the scaffold, were considered.

Data analysis and visualisation.

All statistical analyses were conducted using R v4.1.3 [58]. Viral community alpha (within-sample) diversity was described with Shannon's *H* index computed on vOTU CPM profiles with phyloseq v1.38.0 [86]. Viral community evenness was estimated with Pielou's *J* index. Viral community beta (between-sample) diversity was described by computing a Bray-Curtis dissimilarity matrix from square root transformed vOTU CPM values, and subsequently visualised with non-metric multidimensional scaling (NMDS) ordination using vegan v2.6.2 [87]. The same method was used for microbial community beta diversity, using normalised coverage values. Permutational multivariate analysis of variance (PERMANOVA) tests and Mantel tests were also performed with vegan. Pearson's correlation coefficients and linear regression slopes were calculated with stats v4.2.1. Differential abundance analysis was performed on raw read counts with DESeq2 v1.34.0 [88]. Genome maps in Figure S10 were visualised with gggenes v0.4.1 [89]. Fig. S5B was made with ComplexUpset v1.3.3 [90, 91]. All remaining plots were generated with ggplot2 v3.3.6 [92].

Results

Soil viral communities were structured with soil depth at both the population-level and strain-level.

To investigate viral communities with soil depth, we leveraged a publicly available metagenomic data set sampled from grassland soil in northern California [41]. Soil samples were previously collected at six intervals between 20 cm and 115 cm below the surface, at two sites representing contrasting aboveground vegetation: under a Garry oak tree ("Garry Oak" samples), and neighbouring grassland ("Hilly grassland" samples). In total, 24 assembled metagenomes were used to recover viral populations (vOTUs) using a combination of viral prediction tools. This yielded 10,196 non-redundant vOTUs (> 5 kb), representing 9664 dsDNA viral species and 532 ssDNA viral species (Table S1), with 292 vOTUs (2.9% of total) identified as complete or high-quality viral genomes. The mean vOTU genome length was ~ 12 kb, while 19 vOTUs had genome lengths > 200 kb (largest 415,894 bp) and represented "jumbo phages" [93], of which 18 where classified as high-quality genomes.

To estimate the similarity of recovered vOTUs with all currently available phage genomes [56], shared protein-based classification was performed using vConTACT2 [57] (Fig. S1). The resultant network contained viral clusters (VCs) representing roughly genus-level taxonomic groups (Fig. S1A). There were 4124 (42.7% of total) dsDNA vOTUs and 129 (24.2% of total) ssDNA vOTUs which formed 1310 VCs and 89 VCs, respectively (Table S1). However, only ten VCs included both our vOTUs and phage genomes that had been previously isolated, demonstrating the novel viral taxonomic diversity accessed from subsurface soil in this study. The analysis was expanded to include > 600,000 previously identified environmental viral sequences, using PhageClouds [60]. Our vOTUs had intergenomic distances < 0.21 with only

85 previously discovered viral sequences in public databases (Table S4). Of the 75 viral sequences with available metadata at the time of analysis, 74 were assembled from soil.

While only three jumbo phage vOTUs shared a VC with others (cluster 259), 63 vOTUs < 200 kb shared VCs with jumbo phage vOTUs (hereafter referred to as "jumbo-related" vOTUs). To investigate the diversity of these vOTUs further, we constructed a phylogeny of 24 DNA polymerase genes identified within the genomes of eight jumbo phage vOTUs and six jumbo-related vOTUs (Fig. S2). This revealed that the vOTUs belonged to six distinct phylogenetic groups, which we denoted A-F. Further investigation of the groups with the closest known relatives (groups A, B, and F) identified that the most similar DNA polymerase genes were carried by genomes < 200 kb, therefore representing non-jumbo phages (Fig. S3).

To characterise the role of soil depth in shaping the assembly of viral communities, we assessed population-level viral diversity with soil depth (Fig. 1). This revealed that viral richness (measured through the detection of vOTUs), viral evenness (measured with Pielou's J index), and viral diversity (measured with Shannon's H index) significantly increased with soil depth in Garry Oak (Fig. 1A). In contrast, viral richness decreased with soil depth in Hilly grassland, where no linear relationship was observed with viral evenness and diversity (Fig. 1A). Next, we tested whether soil depth was an ecological driver of viral community composition through NMDS ordination and a PERMANOVA test. Bray-Curtis dissimilarities were structured with soil depth ($R^2 = 0.156$, $F = 7.37$, $p = 0.002$) (Fig. 1B), such that significant distance-decay relationships were observed at both sites (Fig. 1C). Additionally, viral communities were distinct between sites, with aboveground vegetation explaining more than twice the variation as soil depth ($R^2 = 0.399$, $F = 18.8$, $p = 0.001$) (Fig. 1B).

To further contrast soil depth patterns between sites, we assessed viral prevalence to identify populations enriched in either surface or subsurface soil. This determined that viral prevalence was high throughout the soil depth profiles, such that 66.0% and 72.1% of vOTUs were shared

across all samples within Garry Oak and Hilly grassland, respectively (Fig. S4). Nonetheless, differential abundance analysis identified that > 29% of vOTUs were enriched in either surface soil (20 cm) or subsurface soil (40 cm − 115 cm) (Table S1). In comparing the relative abundance of enriched viral populations between the two sites, we found that the vOTUs highly abundant in subsurface soil in one site were consistently lowly abundant throughout the soil depth profile in the other site (Fig. S5A). Subsequently, only 11.7% of depth-enriched viral populations were enriched in both sites, with 64.9% of these populations surface-enriched (Fig. S5B). In fact, subsurface-enriched viral populations in each site were genetically different, as the shared populations represented only 18.5% of subsurface-enriched VCs in Garry Oak (Fig. S1B) and 13.5% in Hilly grassland (Fig. S1C). Together, these results outline the increased distinction of subsurface soil viral communities between sites.

Lastly, we investigated the effect of soil depth in driving patterns of strain-level viral diversity (Fig. 2). To achieve this, consensus sequences were reconstructed for each vOTU in each sample, based on the most common alleles detected across variant sites. Subsequent distance-decay relationships were observed across strains of 69 vOTUs, for which the pairwise ANI between consensus sequences decreased towards 0.95 (the threshold for vOTU clustering) with soil depth (Fig. 2A). To summarise the micro diversity across viral populations of each sample, average nucleotide diversity (π) was assessed. This summarises the frequency of nucleotide differences between the individual strains of a population. π was greatest in surface soil and displayed a non-linear relationship with soil depth (Fig. 2B). As a result, no significant relationship was observed between population-level diversity (i.e., macro diversity) and strain-level diversity (i.e., micro diversity) in either site (Fig. 2C).

Virus-host interactions were diverse with soil depth.

To understand the ecological role of soil viruses with the soil depth gradient, we characterised the interactions between viruses and their microbial host communities (Fig. 3).

348 Strong links were revealed between viruses and microbes by observing significant correlations
349 between their community structures (Fig. S6) and diversities (Fig. S7). To provide further
350 evidence of virus-host linkages, we identified the putative host taxa of vOTUs using a
351 combination of proviral scaffold assessment, CRISPR spacer matches, and *de novo* prediction
352 using a probabilistic model [74]. *Actinomycetota* and *Pseudomonadota* were the most common
353 host phyla (Table S1). Moreover, viruses infecting *Actinomycetota* were dominant members of
354 viral communities throughout the soil depth profile of both sites (Fig. 3A). While the patterns
355 of microbial phyla described using OTUs and MAGs were different, they both demonstrated
356 that *Actinomycetota* abundance increased with depth in Hilly grassland (Fig. 3A).
357 Subsequently, *Actinomycetota* and *Pseudomonadota* hosts were significantly correlated with
358 their infecting viruses in Hilly grassland (Fig. S8).

359 Given that viral replication strategies inform virus-host interactions following infection, we
360 investigated the prevalence of lysogeny with soil depth. In total, 2911 (28.6% of total)
361 temperate viruses were detected. The incidence of lysogeny, as measured by the proportion of
362 detected vOTUs which were identified as temperate, was stable across soil depth (Fig. 3B). In
363 contrast, the relative abundance of temperate viruses varied, such that a positive relationship
364 with soil depth was observed in Hilly grassland (Fig. 3C).

365 In addition to host cell lysis, another fundamental ecological role of viruses is the alteration
366 of host metabolism through the expression of AMGs during infection. We identified 220
367 putative AMGs carried by 181 vOTUs (1.77% of total; Table S5), whose functional annotations
368 included hits to ribosomal proteins (nine genes) and carbohydrate-active enzymes (CAZymes;
369 43 genes). Six jumbo phage vOTUs carried a single AMG each, while the average length of
370 vOTUs carrying multiple AMGs was 29,600 bp. vOTUs carrying AMGs were consistently
371 detected throughout the soil depth profiles, with a small yet statistically significant decrease in

372 incidence with depth in Garry Oak (Fig. 3D). No significant depth relationships were observed
373 for the relative abundance of AMG-carrying vOTUs (Fig. 3E).

374 Further inspection of candidate CAZymes with CD-Search revealed that 36/43 (83.7%)
375 gene products contained conserved protein domains associated with carbohydrate metabolism
376 (Table 1). This included 12 genes with glycoside hydrolase domains, putatively involved in the
377 metabolism of four different carbon sources: glycans (five genes), amylose (two genes),
378 cellulose (two genes), and mannose (one gene). vOTUs carrying CAZymes were dispersed
379 across 21 VCs and 17 singletons in the shared protein network (Fig. S1D). Three quarters of
380 vOTUs carrying CAZymes were lytic and 17/40 (42.5%) had predicted hosts, spanning
381 *Actinomycetota* (20%), *Pseudomonadota* (12.5%), *Acidobacteriota* (5%), *Bacillota* (2.5%),
382 and *Nitrospirota* (2.5%). The vOTUs were detected throughout the two soil depth profiles, at
383 consistently low abundance (Fig. S9).

384 **Virus-host antagonistic co-evolution was dynamic throughout the soil depth profile.**

385 Virus-host interactions can also have implications on the eco-evolutionary dynamics of both
386 viruses and microbes. Thus, to investigate virus-host antagonistic co-evolution throughout the
387 soil depth profile, we detected bacterial anti-phage defence systems and estimated the
388 subsequent selection pressure applied to soil viruses (Fig. 4). More than 75% of microbial
389 community abundance was represented by MAGs carrying at least one complete anti-phage
390 system, with systems involving restriction-modification (RM) being the most common (Fig.
391 4A). Further investigation into the anti-phage system repertoire of MAG communities revealed
392 a significant increase in system diversity with soil depth in both sites (Fig. 4B).

393 To assess the resulting evolutionary pressures on viral populations, we identified viral genes
394 under positive selection using a proportion of non-synonymous to synonymous polymorphism
395 ratio (pN/pS) $>$ 1. This yielded 532 vOTUs carrying 880 genes under positive selection in at

396 least one sample, with nearly half of these genes lacking functional annotations (Table S6).
397 Nonetheless, we were able to identify functions for 30 tail fibre proteins involved in host cell
398 recognition [94, 95], four tape measure proteins involved in virion assembly [96] and genome
399 insertion [97], six ribosomal proteins, and 11 ABC transporters (Table S6). Manual inspection
400 of putative ABC transporter genes with CD-Search indicated the presence of conserved
401 secondary structures for ten of the genes, with five genes containing drug efflux transporter
402 domains (*ccmA*, *drrA*, *MacAB*, *MacB*, *SunT*). Moreover, five vOTUs carrying ABC transporter
403 genes represented high-quality temperate viral genomes, with hits to viral protein families
404 (PHROGs) both upstream and downstream of putative transporter genes (Fig. S10). While only
405 one ABC transporter gene was positively selected in surface soil (20 cm), the remaining ten
406 genes were positively selected in subsurface soil (40 cm – 115 cm). Overall, the number of
407 vOTUs carrying at least one gene under positive selection increased with soil depth in Hilly
408 grassland, while a non-linear relationship was observed with soil depth in Garry Oak (Fig. 4C).
409

410 ## Discussion

411 **High viral dispersal maintains virus-host co-existence throughout the soil depth profile.**

412 Microbial dispersal underpins soil ecology and evolution [98], however we lack
413 understanding of the distribution patterns of soil viruses. In this study, we observed high viral
414 prevalence throughout two soil depth profiles, with more than two thirds of viral populations
415 detected in every soil sample (Fig. S4). This cosmopolitan distribution contrasted with recent
416 investigations of soil viral dispersal, in which fewer viruses were shared between samples
417 across horizontal [14, 16, 17, 99, 100] and vertical space [18, 99, 101]. Despite high viral
418 prevalence, we discovered that soil depth shaped the composition of viral communities (Fig.
419 1B), such that viral community diversity displayed a distance-decay relationship (Fig. 1C).

The structuring of viral communities with soil depth is undoubtedly driven by the physical structure of the soil matrix, which renders virion dispersal a mostly stochastic process [98]. The rate-limiting factors underlying the transport of viruses through soil are likely different to those of their hosts [32, 102]. Notably, soil viruses are expected to be passively distributed with water more easily [103]. Therefore, wetter soils may facilitate the enhanced mobility of viruses compared to their hosts, resulting in the increased accessibility and infection of susceptible host cells. Simultaneously, the abundance of viruses are also correlated with soil moisture content [14, 16, 17, 99], demonstrating how environmental factors may affect virus-host interactions.

At the Sagehorn site where soil samples were taken, significant winter precipitation raises the water table close to the soil surface [104]. The resulting annual saturation of soil may facilitate the immigration of infective viruses and susceptible hosts throughout the soil depth profile. This would have consequences on both viral and bacterial persistence due to evolutionary "source-sink dynamics", where co-existence is maintained by the heterogeneous distribution of viruses and hosts [105, 106]. This has been demonstrated in biofilm simulations, whereby the mobility of viruses is a key determinant of phage-bacteria co-existence [107]. Therefore, we propose that the high viral dispersal is likely to have implications on the eco-evolutionary interactions occurring across the soil niches examined in this study.

Tree association impacts viral community composition in both surface and subsurface soil.

Intriguingly, the variation in viral communities between sites was greater than the variation associated with soil depth, such that communities in subsurface soils were more distinct than those at the surface (Fig. 1B). A considerable distinction between the two sites was the presence of Garry Oak trees. At the Garry Oak site, the tree canopy could have provided the soil surface with protection from the sun, potentially maintaining greater soil moisture content as compared

445 to the unshaded soil in Hilly grassland. While changes to moisture content would be likely to
446 affect viral dispersal and the structuring of soil viral communities, no soil property
447 measurements were available to confirm this hypothesis.

448 Another consequence of Garry Oak trees is the annual shedding of leaves during winter
449 [46]. Decaying leaf litter has been shown to shape the composition of RNA viral communities
450 in both the rhizosphere and bulk soil [108]. While quicker degradation rates mean that the
451 spatial structuring of RNA viruses may be greater than for DNA viruses, the legacy effects of
452 leaf litter may have driven differences between surface soils. However, the degradation of shed
453 leaves would be expected to have less impact on subsurface communities. Instead, we
454 hypothesise that the presence of tree roots and the associated fungal hyphae impact viral
455 communities in Garry Oak samples, leading to the discrepancies in the depth patterns between
456 the two sites. Indeed, fine roots and hyphae have been reported to a depth of at least 2 m at the
457 same study site [46]. The consequence of growing crop roots on the structures of both DNA
458 and RNA soil viral communities has been demonstrated previously [13].

459 **The prevalence of lysogeny was consistent throughout the soil depth profile.**

460 Lysogenic viral infections can have significant eco-evolutionary impacts on host
461 communities [30], most notably through superinfection exclusion, which confers resistance
462 against further viral infection [109–111]. Typically, lysogeny is expected to dominate in soil
463 ecosystems because of low host biomass and viability [28, 29, 35]. Under low bacterial
464 densities (e.g., $< 10^5$ cells per gram), host starvation represses viral lytic genes through ATP-
465 dependant signalling cascades [112, 113], promoting lysogeny switching [114]. Subsequently,
466 lower bacterial abundances have been associated with increased lysogeny in the deep ocean
467 [115–117]. Recent work has observed an increased prevalence of lysogeny in subsurface soils,
468 as detected through inducible lysogens [28], however we observed very little change in the
469 incidence of temperate viruses across soil depth (Fig. 3B). And while the relative abundance

of temperate phages did increase with soil depth in Hilly grassland, this was not consistent in Garry Oak (Fig. 3C). Therefore, there could be additional factors which govern lysogeny switching in soils beyond host density. This could include non-linear relationships with host metabolism [114], viral-viral interactions [118, 119], and anti-phage defence systems [85]. To this point, the diversity of anti-phage defence systems was enriched among subsurface communities in Hilly grassland (Fig. 4B), coinciding with the increased abundance of temperate viruses. The increased encountering of lysogenic infection mechanisms may have been responsible for the greater range of defence systems maintained among the host community [85]. It must also be noted that viruses without lysogenic genes can establish passive co-existence typified by temperate lifestyles, as demonstrated with ΦcrAss001 in continuous culture with its host Bacteroides intestinalis [120]. Therefore, non-lysogenic phages may be able to replicate without eradicating their host population, in contrast to the traditional view of predator-prey cycles induced by lytic phages.

Jumbo phages recovered from soil were polyphyletic.

We recovered 19 vOTUs representing jumbo phages [93] with genome lengths > 200 kb (largest 415,894 bp), without implementing a viral contig binning approach. An additional 63 vOTUs formed roughly genus-level VCs with jumbo phages, and together they represented six distinct clades based on DNA polymerase gene phylogeny (Fig. S2). This is consistent with previous findings that jumbo phages are polyphyletic, implying that phage genome gigantism has evolved numerous times instead of originating from a single common ancestor [121, 122]. Furthermore, the phylogeny revealed that the closest known relatives to jumbo phage vOTUs had much shorter genomes (Fig. S3). It has been postulated that jumbo phages may have evolved from recombination events between multiple smaller phage genomes [121]. Another potential hypothesis for the origin of phage genome gigantism is that the genomes could have expanded upon the acquisition of additional phage or host genes. The ratchet model describes

how mutations that increase the capsid size facilitate the acquisition of new viral genes, which are then stable against loss of function mutations [123].

Previously identified clades of jumbo phages have been discerned by their diverse infection and replication strategies, biogeography, and host taxa [121, 122]. We have uncovered the ubiquity of jumbo phages across soil depth, suggesting that large genome sizes are evolutionarily stable across both surface and subsurface soil niches. Furthermore, jumbo phages were consistently in the top 20% of the most abundant viruses in each community (Fig. S11), contrasting with previous findings that giant viruses (> 300kb) are lowly abundant in forest soil [124].

Soil viruses augment microbial metabolism in subsurface soils.

Viruses can carry and express AMGs during infection to modulate the host's metabolism and fitness, and promote their co-existence [2–6]. Moreover, viral-encoded AMGs have the potential to affect soil biogeochemistry, with viruses previously implicated in soil carbon processing [13, 18, 19, 34, 99, 125]. In this study, we detected viruses throughout the soil depth profile carrying CAZymes associated with both carbohydrate anabolism and catabolism (Table S5). The rank abundance of CAZyme-carrying viruses was highly variable, but their presence was ubiquitous across all soil depths (Fig. S12). Therefore, soil viruses may stimulate the degradation of a variety of carbon sources, including plant cell walls, thus contributing to the remineralisation of soil carbon in surface and subsurface soil. While our discovery of viral CAZymes adds to the repertoire of potential viral mechanisms contributing to soil carbon cycling, evidence of their function during the infection cycle has not been confirmed here.

Previously, the abundance of viral-encoded AMGs was found to increase with soil depth [101]. However, we observed that the abundance of viruses carrying AMGs was consistently low throughout both soil depth profiles (Fig. 3D-E). The most common host phyla of viruses

519 carrying AMGs was *Actinomycetota*, for which both the host (Fig. 3A) and infecting viruses
520 (Fig. S13) were more abundant in subsurface soil. *Actinomycetota* (formerly *Actinobacteria*)
521 are dominant soil microbes [126] and contribute to soil carbon cycling by producing
522 extracellular hydrolytic enzymes which depolymerise plant-derived lignin [127]. Furthermore,
523 *Actinomycetota* are resilient to soil drying, such that their relative abundance increases during
524 drought and declines in the days following re-wetting [128–130]. The abundance and activity
525 blooms in response to seasonal wetting and drying are likely to affect soil nutrient and carbon
526 cycling [130].

527 **Viral macro diversity and micro diversity were associated in surface soil only.**

528 The evolution of viral communities can be monitored through micro diversity. In this study,
529 we have revealed patterns of viral micro diversity across a soil environmental gradient for the
530 first time. Viral strain-level heterogeneity displayed a distance-decay relationship (Fig. 2A)
531 and the average micro diversity (π) of viral communities varied across space (Fig. 2B).

532 Micro diversity is accrued through *de novo* mutations, and can drive phenotypic variation
533 to specialise organisms to their environment [83]. More specifically for viruses, micro diversity
534 reflects evolutionary responses to host infection dynamics, and is directly related to viral
535 infection rates. Greater viral micro diversity, as measured by larger π values, can arise in
536 multiple ways [81]. Firstly, the active infection of hosts can result in population expansion and
537 thus more frequent mutations. This can be exacerbated through genetic recombination between
538 viral populations co-infecting the same host. Such horizontal gene transfer events are made
539 more likely by the presence of microbial "hotspots" occurring throughout the spatially
540 structured soil matrix [131]. Secondly, viral populations could maintain greater micro diversity
541 in their populations as an evolutionary mechanism. Genetic diversity increases the fitness of a
542 viral population by allowing them to "bet-hedge" if their environment or host changes,
543 conferring local adaptation [132].

The ecological forces driving strain-level variation were distinct from those driving population-level variation, as demonstrated by their non-significant association (Fig. 2C). This was surprising given that genetic heterogeneity between strains can result in speciation events [132, 133], thus relating the two levels of diversity. Throughout ocean depth profiles, a similar absent relationship was explained by interactions with bacterial macro diversity [82]. However, no such relationship was observed in these soil samples (Fig. S14). We speculate that unmeasured physicochemical properties, distinct between soil horizons, may have driven the non-linear diversity dynamics we observed throughout the soil depth profile.

Interestingly, when the analysis of viral diversity patterns was focussed on the top 60 cm of soil, viral macro diversity was negatively associated with viral micro diversity (Fig. 2B). This could have resulted from decreasing host cell density from surface to subsurface soil [26], which favours inter-specific viral competition (i.e., reflected in macro diversity) over intra-specific viral competition (i.e., reflected in micro diversity). Hence, strain-level heterogeneity is less favoured when fewer hosts are available, during which species-level competition drives evolution. This would be expected to impact virus-host interactions by reducing the resilience of the subsurface soil niche.

Antagonistic co-evolution was distinct among surface and subsurface communities.

Host defence responses to viral infection are expected to drive positive selection among soil viruses through antagonistic co-evolution. To this aim, we identified 880 viral genes under positive selection (Table S6), for which non-synonymous polymorphisms were more likely to be retained than rejected. This included 30 tail fibre genes, which have previously been shown to be positively selected among gut phages as evidence of their adaptive evolution [134, 135]. Phage tail fibre proteins are involved in host tropism [94, 95], thus the carriage of genetically diverse tail fibre genes may expand a population's host range. Given the positive selection of

568 tail fibre gene mutants throughout the soil depth profile, the evolutionary benefit of expanding
569 host range was universal among viruses occupying both surface and subsurface soil niches.

570 We also identified 11 ABC transporter genes under positive selection, predominantly in
571 subsurface soil (40 cm – 115 cm) (Table S6). Five vOTUs carrying ABC transporter genes
572 represented high-quality temperate viral genomes (Fig. S10), with two of these genes sharing
573 conserved protein domains with ABC drug efflux transporters. By expressing these genes
574 during infection, temperate soil viruses may confer antibiotic resistance to their hosts, thus
575 maintaining their mutual co-existence. Furthermore, the evidence of adaptive evolution among
576 these genes indicates that there is a selection pressure on these viruses to augment their host's
577 interbacterial competition. While this may be the first evidence of soil viruses carrying ABC
578 transporters, the expression of phosphate-binding *pstS* genes by cyanophages has implicated
579 marine viruses in enhancing phosphate uptake in cyanobacterial hosts [136]. Many other viral
580 genes under positive selection had no functional annotation, suggesting that we may be missing
581 alternative selection pressures on soil viruses. For example, missing annotations may include
582 uncharacterised anti-defence proteins, expressed by viruses to target host defence systems and
583 maintain infective capabilities [137].

584 To characterise the range of host defence responses to viral infection, we identified anti-
585 phage defence systems within microbial MAGs. The relative abundance of MAGs adopting at
586 least one system was high throughout the soil depth profile (Fig. 4A), and the increasing
587 diversity of anti-phage systems (Fig. 4B) suggested that the antagonistic co-evolution
588 landscape differed between surface and subsurface niches. Multiple anti-phage defence
589 systems can be carried within defence islands [138], a genetic toolbox of diverse mechanisms
590 to resist viral infection, presumably accrued through horizontal gene transfer events [137]. The
591 genetic diversity of infecting viruses can direct the evolution of host defence strategies, such
592 that low viral diversity may favour CRISPR-based immunity, while higher viral diversity

promotes surface modification mechanisms [139]. Thus, the microheterogeneity driven by the soil matrix would make these virus-host interactions difficult to predict.

Conclusions

Most soil viral ecology efforts have focussed on the top 20 cm of soil, hindering our understanding of subsurface viruses. Given the exponential decay in microbial biomass with soil depth, one might expect relatively minimal ecological impacts of subsurface viral communities. To the contrary, we have uncovered evidence of soil viruses contributing to terrestrial ecology in both surface and subsurface soil niches. The prevalence of lysogeny was consistent throughout the soil depth profile, indicating that additional factors beyond host cell density may govern lysogeny switching in soils. By investigating patterns of viral micro diversity across a soil environmental gradient for the first time, we revealed that the local adaptation of viruses was greatest in surface soil. Furthermore, an increasing diversity of anti-phage defence systems with depth suggests that the antagonistic co-evolution landscape is distinct in subsurface soil. In the future, we predict that comparative activity studies, contrasting surface and subsurface niches, will be essential to characterise viral functions associated with soil depth.

Abbreviations

AMG: Auxiliary Metabolic Gene; CAZyme: Carbohydrate-Active enZymes; CD-Search: Conserved Domain Search; CPM: Counts Per kilobase Million; dsDNA: double-stranded DNA; kb: kilobases; MAG: Metagenome-Assembled Genome; NMDS: Non-metric Multi-Dimensional Scaling; OTU: Operational Taxonomic Unit; PERMANOVA: PERmutational

Multivariate ANalysis Of VAriances; pN/pS: proportion of Non-synonymous to Synonymous polymorphism ratio; RM: Restriction Modification; rpS3: ribosomal protein S3; ssDNA: single-stranded DNA; VC: Viral Cluster; vOTU: Viral Operational Taxonomic Unit.

Declarations

Ethics approval and consent to participate

Not applicable.

Consent for publication

Not applicable.

Availability of data and materials

The metagenomic data set can be accessed from NCBI under project accession PRJNA577476 (sample accessions SAMN13153360-SAMN13153383). DNA vOTU genome sequences were deposited to the European Nucleotide Archive (ENA) under project accession PRJEB57765 (sample accession SAMEA112154074). FASTA nucleotide files containing vOTU genomes, FASTA amino acid files containing vOTU genes, vOTU gene annotations, vConTACT2 network input and output files, rpS3 protein sequences, and assembled MAG sequences are available from figshare (https://figshare.com/XXX). The custom R script used to generate figures and tables, along with required input files, are available from GitHub (https://github.com/GeorgeMuscatt/GrasslandDepthVirome).

Competing interests

The authors declare that they have no competing interests.

Funding

G.M. was funded by the EPSRC & BBSRC Centre for Doctoral Training in Synthetic Biology grant EP/L016494/1. A.M. was funded by MRC grants MR/L015080/1 and

639 MR/T030062/1. G.B. was funded by BBSRC grant BB/L025892/1. E.J. was funded by
640 Warwick Integrative Synthetic Biology (WISB), supported jointly by BBSRC & EPSRC, grant
641 BB/M017982/1.

642 **Authors' contributions**

643 G.M., A.M., G.D.B. and E.J. conceived and designed the analyses. G.M. accessed the data
644 set, carried out bioinformatic analyses, generated R scripts, interpreted data, prepared figures,
645 and produced the first draft of the manuscript. R.C. aided with bioinformatic analyses. A.M.,
646 G.D.B., and E.J. provided edits and additional contributions to the manuscript. All authors read
647 and approved the final submitted manuscript.

648 **Acknowledgements**

649 We would like to thank the authors of Sharrar et al. [41] for performing sampling and
650 sequencing, and for making the soil metagenomes and associated metadata publicly available.
651 We acknowledge the use of MRC-CLIMB for the provision of high-performance servers,
652 without which this work wouldn't be possible.

653

References

1. Gougoulias C, Clark JM, Shaw LJ. The role of soil microbes in the global carbon cycle: tracking the below-ground microbial processing of plant-derived carbon for manipulating carbon dynamics in agricultural systems. J Sci Food Agric. 2014;94:2362–71.

2. Aylward FO, Boeuf D, Mende DR, Wood-Charlson EM, Vislova A, Eppley JM, et al. Diel cycling and long-term persistence of viruses in the ocean's euphotic zone. Proc Natl Acad Sci. 2017;114:11446–51.

3. Lindell D, Jaffe JD, Coleman ML, Futschik ME, Axmann IM, Rector T, et al. Genome-wide expression dynamics of a marine virus and host reveal features of co-evolution. Nature. 2007;449:83–6.

4. Puxty RJ, Evans DJ, Millard AD, Scanlan DJ. Energy limitation of cyanophage development: implications for marine carbon cycling. ISME J. 2018;12:1273–86.

5. Zeng Q, Chisholm SW. Marine viruses exploit their host's two-component regulatory system in response to resource limitation. Curr Biol. 2012;22:124–8.

6. Puxty RJ, Millard AD, Evans DJ, Scanlan DJ. Viruses inhibit CO2 fixation in the most abundant phototrophs on earth. Curr Biol. 2016;26:1585–9.

7. Suttle CA. Marine viruses — major players in the global ecosystem. Nat Rev Microbiol. 2007;5:801–12.

8. Breitbart M, Bonnain C, Malki K, Sawaya NA. Phage puppet masters of the marine microbial realm. Nat Microbiol. 2018;3:754–66.

9. Weitz JS, Stock CA, Wilhelm SW, Bourouiba L, Coleman ML, Buchan A, et al. A multitrophic model to quantify the effects of marine viruses on microbial food webs and ecosystem processes. ISME J. 2015;9:1352–64.

10. Göller PC, Haro-Moreno JM, Rodriguez-Valera F, Loessner MJ, Gómez-Sanz E. Uncovering a hidden diversity: optimized protocols for the extraction of dsDNA bacteriophages from soil. Microbiome. 2020;8:17.

11. Trubl G, Hyman P, Roux S, Abedon ST. Coming-of-age characterization of soil viruses: a user's guide to virus isolation, detection within metagenomes, and viromics. Soil Syst. 2020;4:23.

12. Trubl G, Roux S, Solonenko N, Li Y-F, Bolduc B, Rodríguez-Ramos J, et al. Towards optimized viral metagenomes for double-stranded and single-stranded DNA viruses from challenging soils. PeerJ. 2019;7:e7265.

13. Muscatt G, Hilton S, Raguideau S, Teakle G, Lidbury IDEA, Wellington EMH, et al. Crop management shapes the diversity and activity of DNA and RNA viruses in the rhizosphere. Microbiome. 2022;10:181.

14. Durham DM, Sieradzki ET, ter Horst AM, Santos-Medellín C, Bess CWA, Geonczy SE, et al. Substantial differences in soil viral community composition within and among four Northern California habitats. preprint. Microbiology; 2022.

15. Hillary LS, Adriaenssens EM, Jones DL, McDonald JE. RNA-viromics reveals diverse communities of soil RNA viruses with the potential to affect grassland ecosystems across multiple trophic levels. ISME Commun. 2022;2:34.

16. Santos-Medellín C, Zinke LA, ter Horst AM, Gelardi DL, Parikh SJ, Emerson JB. Viromes outperform total metagenomes in revealing the spatiotemporal patterns of agricultural soil viral communities. ISME J. 2021. https://doi.org/10.1038/s41396-021-00897-y.

17. Santos-Medellín C, Estera-Molina K, Yuan M, Pett-Ridge J, Firestone MK, Emerson JB. Spatial turnover of soil viral populations and genotypes overlain by cohesive responses to moisture in grasslands. Proc Natl Acad Sci. 2022;119:e2209132119.

18. ter Horst AM, Santos-Medellín C, Sorensen JW, Zinke LA, Wilson RM, Johnston ER, et al. Minnesota peat viromes reveal terrestrial and aquatic niche partitioning for local and global viral populations. Microbiome. 2021;9:233.

19. Bi L, Yu D, Du S, Zhang L, Zhang L, Wu C, et al. Diversity and potential biogeochemical impacts of viruses in bulk and rhizosphere soils. Environ Microbiol. 2021;23:588–99.

20. Rumpel C, Kögel-Knabner I. Deep soil organic matter—a key but poorly understood component of terrestrial C cycle. Plant Soil. 2011;338:143–58.

21. Bardgett RD, Freeman C, Ostle NJ. Microbial contributions to climate change through carbon cycle feedbacks. ISME J. 2008;2:805–14.

22. Singh BK, Bardgett RD, Smith P, Reay DS. Microorganisms and climate change: terrestrial feedbacks and mitigation options. Nat Rev Microbiol. 2010;8:779–90.

23. Rodríguez-Cruz M, Jones JE, Bending GD. Field-scale study of the variability in pesticide biodegradation with soil depth and its relationship with soil characteristics. Soil Biol Biochem. 2006;38:2910–8.

24. Jiao S, Chen W, Wang J, Du N, Li Q, Wei G. Soil microbiomes with distinct assemblies through vertical soil profiles drive the cycling of multiple nutrients in reforested ecosystems. Microbiome. 2018;6:146.

25. Stone MM, DeForest JL, Plante AF. Changes in extracellular enzyme activity and microbial community structure with soil depth at the Luquillo Critical Zone Observatory. Soil Biol Biochem. 2014;75:237–47.

26. Eilers KG, Debenport S, Anderson S, Fierer N. Digging deeper to find unique microbial communities: the strong effect of depth on the structure of bacterial and archaeal communities in soil. Soil Biol Biochem. 2012;50:58–65.

27. Fierer N, Schimel JP, Holden PA. Variations in microbial community composition through two soil depth profiles. Soil Biol Biochem. 2003;35:167–76.

28. Liang X, Zhang Y, Wommack KE, Wilhelm SW, DeBruyn JM, Sherfy AC, et al. Lysogenic reproductive strategies of viral communities vary with soil depth and are correlated with bacterial diversity. Soil Biol Biochem. 2020;144:107767.

29. Williamson KE, Radosevich M, Smith DW, Wommack KE. Incidence of lysogeny within temperate and extreme soil environments. Environ Microbiol. 2007;9:2563–74.

30. Howard-Varona C, Hargreaves KR, Abedon ST, Sullivan MB. Lysogeny in nature: mechanisms, impact and ecology of temperate phages. ISME J. 2017;11:1511–20.

31. Ghosh D, Roy K, Williamson KE, White DC, Wommack KE, Sublette KL, et al. Prevalence of lysogeny among soil bacteria and presence of 16S rRNA and trzN genes in viral-community DNA. Appl Environ Microbiol. 2008;74:495–502.

32. Kimura M, Jia Z-J, Nakayama N, Asakawa S. Ecology of viruses in soils: past, present and future perspectives. Soil Sci Plant Nutr. 2008;54:1–32.

738 33. Stewart FM, Levin BR. The population biology of bacterial viruses: why be temperate.
739 Theor Popul Biol. 1984;26:93–117.

740 34. Trubl G, Jang HB, Roux S, Emerson JB, Solonenko N, Vik DR, et al. Soil viruses are
741 underexplored players in ecosystem carbon processing. mSystems. 2018;3:e00076-18,
742 /msystems/3/5/msys.00076-18.atom.

743 35. Zablocki O, Adriaenssens EM, Cowan D. Diversity and ecology of viruses in hyperarid
744 desert soils. Appl Environ Microbiol. 2016;82:770–7.

745 36. Paterson S, Vogwill T, Buckling A, Benmayor R, Spiers AJ, Thomson NR, et al.
746 Antagonistic coevolution accelerates molecular evolution. Nature. 2010;464:275–8.

747 37. Gómez P, Buckling A. Bacteria-phage antagonistic coevolution in soil. Science.
748 2011;332:106–9.

749 38. Betts A, Gray C, Zelek M, MacLean RC, King KC. High parasite diversity accelerates host
750 adaptation and diversification. Science. 2018;360:907–11.

751 39. Larsen ML, Wilhelm SW, Lennon JT. Nutrient stoichiometry shapes microbial
752 coevolution. Ecol Lett. 2019;22:1009–18.

753 40. Jover LF, Effler TC, Buchan A, Wilhelm SW, Weitz JS. The elemental composition of
754 virus particles: implications for marine biogeochemical cycles. Nat Rev Microbiol.
755 2014;12:519–28.

756 41. Sharrar AM, Crits-Christoph A, Méheust R, Diamond S, Starr EP, Banfield JF. Bacterial
757 secondary metabolite biosynthetic potential in soil varies with phylum, depth, and
758 vegetation type. mBio. 2020;11:e00416-20.

759 42. White RP, Murray S, Rohweder M. Pilot analysis of global ecosystems: grassland
760 ecosystems. Washington, DC: World Resources Institute; 2000.

761 43. Eze S, Palmer SM, Chapman PJ. Soil organic carbon stock in grasslands: effects of
762 inorganic fertilizers, liming and grazing in different climate settings. J Environ Manage.
763 2018;223:74–84.

764 44. Zhao Y, Liu Z, Wu J. Grassland ecosystem services: a systematic review of research
765 advances and future directions. Landsc Ecol. 2020;35:793–814.

766 45. Blake Jr. MC, Jones DL. Origin of franciscan melanges in northern California. SEPM Spec
767 Publ. 1974;:345–57.

768 46. Hahm WJ, Dietrich WE, Dawson TE. Controls on the distribution and resilience of *Quercus*
769 *garryana*: ecophysiological evidence of oak's water-limitation tolerance. Ecosphere.
770 2018;9.

771 47. Ren J, Song K, Deng C, Ahlgren NA, Fuhrman JA, Li Y, et al. Identifying viruses from
772 metagenomic data using deep learning. Quant Biol. 2020;8:64–77.

773 48. Kieft K, Zhou Z, Anantharaman K. VIBRANT: automated recovery, annotation and
774 curation of microbial viruses, and evaluation of viral community function from genomic
775 sequences. Microbiome. 2020;8:90.

776 49. Guo J, Bolduc B, Zayed AA, Varsani A, Dominguez-Huerta G, Delmont TO, et al.
777 VirSorter2: a multi-classifier, expert-guided approach to detect diverse DNA and RNA
778 viruses. Microbiome. 2021;9:37.

779 50. Nayfach S, Camargo AP, Schulz F, Eloe-Fadrosh E, Roux S, Kyrpides NC. CheckV
780 assesses the quality and completeness of metagenome-assembled viral genomes. Nat
781 Biotechnol. 2021;39:578–85.

782 51. Shaffer M, Borton MA, McGivern BB, Zayed AA, La Rosa SL, Solden LM, et al. DRAM
783 for distilling microbial metabolism to automate the curation of microbiome function.
784 Nucleic Acids Res. 2020;48:8883–900.

785 52. Guo J, Vik D, Adjie Pratama A, Roux S, Sullivan M. Viral sequence identification SOP
786 with VirSorter2 v3. 2021.

787 53. Roux S, Adriaenssens EM, Dutilh BE, Koonin EV, Kropinski AM, Krupovic M, et al.
788 Minimum information about an uncultivated virus genome (MIUViG). Nat Biotechnol.
789 2019;37:29–37.

790 54. Seemann T. Prokka: rapid prokaryotic genome annotation. Bioinformatics. 2014;30:2068–
791 9.

792 55. Terzian P, Olo Ndela E, Galiez C, Lossouarn J, Pérez Bucio RE, Mom R, et al. PHROG:
793 families of prokaryotic virus proteins clustered using remote homology. NAR Genomics
794 Bioinforma. 2021;3:lqab067.

795 56. Cook R, Brown N, Redgwell T, Rihtman B, Barnes M, Clokie M, et al. Infrastructure for a
796 phage reference database: identification of large-scale biases in the current collection of
797 cultured phage genomes. PHAGE. 2021;2:214–23.

798 57. Bin Jang H, Bolduc B, Zablocki O, Kuhn JH, Roux S, Adriaenssens EM, et al. Taxonomic
799 assignment of uncultivated prokaryotic virus genomes is enabled by gene-sharing networks.
800 Nat Biotechnol. 2019;37:632–9.

801 58. R Core Team. R: a language and environment for statistical computing. Vienna, Austria: R
802 Foundation for Statistical Computing; 2021.

803 59. Schloerke B, Cook D, Larmarange J, Briatte F, Marbach M, Thoen E, et al. GGally:
804 extension to "ggplot2." 2021.

805 60. Rangel-Pineros G, Millard A, Michniewski S, Scanlan D, Sirén K, Reyes A, et al. From
806 trees to clouds: PhageClouds for fast comparison of ~640,000 phage genomic sequences
807 and host-centric visualization using genomic network graphs. PHAGE. 2021;2:194–203.

808 61. Edgar RC. Search and clustering orders of magnitude faster than BLAST. Bioinformatics.
809 2010;26:2460–1.

810 62. Katoh K. MAFFT: a novel method for rapid multiple sequence alignment based on fast
811 Fourier transform. Nucleic Acids Res. 2002;30:3059–66.

812 63. Katoh K, Standley DM. MAFFT multiple sequence alignment software version 7:
813 improvements in performance and usability. Mol Biol Evol. 2013;30:772–80.

814 64. Nguyen L-T, Schmidt HA, von Haeseler A, Minh BQ. IQ-TREE: a fast and effective
815 stochastic algorithm for estimating maximum-likelihood phylogenies. Mol Biol Evol.
816 2015;32:268–74.

817 65. Minh BQ, Schmidt HA, Chernomor O, Schrempf D, Woodhams MD, von Haeseler A, et
818 al. IQ-TREE 2: new models and efficient methods for phylogenetic inference in the genomic
819 era. Mol Biol Evol. 2020;37:1530–4.

820 66. Hoang DT, Chernomor O, von Haeseler A, Minh BQ, Vinh LS. UFBoot2: improving the
821 ultrafast bootstrap approximation. Mol Biol Evol. 2018;35:518–22.

822 67. Yu G. Using ggtree to visualize data on tree-like structures. Curr Protoc Bioinforma.
823 2020;69.

824 68. Yu G, Lam TT-Y, Zhu H, Guan Y. Two methods for mapping and visualizing associated
825 data on phylogeny using ggtree. Mol Biol Evol. 2018;35:3041–3.

826 69. Yu G, Smith DK, Zhu H, Guan Y, Lam TT. ggtree: an R package for visualization and
827 annotation of phylogenetic trees with their covariates and other associated data. Methods
828 Ecol Evol. 2017;8:28–36.

829 70. Babenko VV, Millard A, Kulikov EE, Spasskaya NN, Letarova MA, Konanov DN, et al.
830 The ecogenomics of dsDNA bacteriophages in feces of stabled and feral horses. Comput
831 Struct Biotechnol J. 2020;18:3457–67.

832 71. Cook R, Hooton S, Trivedi U, King L, Dodd CER, Hobman JL, et al. Hybrid assembly of
833 an agricultural slurry virome reveals a diverse and stable community with the potential to
834 alter the metabolism and virulence of veterinary pathogens. Microbiome. 2021;9:65.

835 72. Edgar RC. PILER-CR: Fast and accurate identification of CRISPR repeats. BMC
836 Bioinformatics. 2007;8:18.

837 73. Dion MB, Plante P-L, Zufferey E, Shah SA, Corbeil J, Moineau S. Streamlining CRISPR
838 spacer-based bacterial host predictions to decipher the viral dark matter. Nucleic Acids Res.
839 2021;49:3127–38.

840 74. Galiez C, Siebert M, Enault F, Vincent J, Söding J. WIsH: who is the host? Predicting
841 prokaryotic hosts from metagenomic phage contigs. Bioinformatics. 2017;33:3113–4.

842 75. Pratama AA, Bolduc B, Zayed AA, Zhong Z-P, Guo J, Vik DR, et al. Expanding standards
843 in viromics: *in silico* evaluation of dsDNA viral genome identification, classification, and
844 auxiliary metabolic gene curation. PeerJ. 2021;9:e11447.

845 76. Marchler-Bauer A, Bryant SH. CD-Search: protein domain annotations on the fly. Nucleic
846 Acids Res. 2004;32 Web Server:W327–31.

847 77. Lu S, Wang J, Chitsaz F, Derbyshire MK, Geer RC, Gonzales NR, et al. CDD/SPARCLE:
848 the conserved domain database in 2020. Nucleic Acids Res. 2020;48:D265–8.

849 78. Bushnell B. BBMap: a fast, accurate, splice-aware aligner. Lawrence Berkeley National
850 Lab.(LBNL), Berkeley, CA (United States); 2014.

851 79. Roux S, Emerson JB, Eloe-Fadrosh EA, Sullivan MB. Benchmarking viromics: an *in silico*
852 evaluation of metagenome-enabled estimates of viral community composition and diversity.
853 PeerJ. 2017;5:e3817.

854 80. Hug LA, Baker BJ, Anantharaman K, Brown CT, Probst AJ, Castelle CJ, et al. A new view
855 of the tree of life. Nat Microbiol. 2016;1:16048.

856 81. Gregory AC, Gerhardt K, Zhong Z-P, Bolduc B, Temperton B, Konstantinidis KT, et al.
857 MetaPop: a pipeline for macro- and microdiversity analyses and visualization of microbial
858 and viral metagenome-derived populations. Microbiome. 2022;10:49.

859 82. Gregory AC, Zayed AA, Conceição-Neto N, Temperton B, Bolduc B, Alberti A, et al.
860 Marine DNA viral macro- and microdiversity from pole to pole. Cell. 2019;177:1109-
861 1123.e14.

862 83. Olm MR, Crits-Christoph A, Bouma-Gregson K, Firek BA, Morowitz MJ, Banfield JF.
863 inStrain profiles population microdiversity from metagenomic data and sensitively detects
864 shared microbial strains. Nat Biotechnol. 2021;39:727–36.

865 84. Abby SS, Néron B, Ménager H, Touchon M, Rocha EPC. MacSyFinder: a program to mine
866 genomes for molecular systems with an application to CRISPR-Cas systems. PLoS ONE.
867 2014;9:e110726.

868 85. Tesson F, Hervé A, Mordret E, Touchon M, d'Humières C, Cury J, et al. Systematic and
869 quantitative view of the antiviral arsenal of prokaryotes. Nat Commun. 2022;13:2561.

870 86. McMurdie PJ, Holmes S. Phyloseq: an R package for reproducible interactive analysis and
871 graphics of microbiome census data. PLoS ONE. 2013;8:e61217.

872 87. Oksanen J, Blanchet FG, Friendly M, Kindt R, Legendre P, McGlinn D, et al. vegan:
873 community ecology package. 2020.

874 88. Love MI, Huber W, Anders S. Moderated estimation of fold change and dispersion for
875 RNA-seq data with DESeq2. Genome Biol. 2014;15:550.

876 89. Wilkins D. gggenes: Draw Gene Arrow Maps in "ggplot2." 2020.

877 90. Lex A, Gehlenborg N, Strobelt H, Vuillemot R, Pfister H. UpSet: Visualization of
878 Intersecting Sets. IEEE Trans Vis Comput Graph. 2014;20:1983–92.

879 91. Krassowski M, Arts M, Lagger C. krassowski/complex-upset: v1.3.3. 2021.

880 92. Wickham H. ggplot2: elegant graphics for data analysis. Springer-Verlag New York; 2016.

881 93. Yuan Y, Gao M. Jumbo bacteriophages: an overview. Front Microbiol. 2017;8.

882 94. Scholl D, Rogers S, Adhya S, Merril CR. Bacteriophage K1-5 encodes two different tail
883 fiber proteins, allowing it to infect and replicate on both K1 and K5 strains of *Escherichia*
884 *coli*. J Virol. 2001;75:2509–15.

885 95. Tétart F, Repoila F, Monod C, Krisch HM. Bacteriophage T4 host range is expanded by
886 duplications of a small domain of the tail fiber adhesin. J Mol Biol. 1996;258:726–31.

887 96. Mahony J, Alqarni M, Stockdale S, Spinelli S, Feyereisen M, Cambillau C, et al. Functional
888 and structural dissection of the tape measure protein of lactococcal phage TP901-1. Sci Rep.
889 2016;6:36667.

890 97. Cumby N, Reimer K, Mengin-Lecreulx D, Davidson AR, Maxwell KL. The phage tail tape
891 measure protein, an inner membrane protein and a periplasmic chaperone play connected
892 roles in the genome injection process of *E. coli* phage HK97: Phage and host protein
893 requirements for HK97 genome injection. Mol Microbiol. 2015;96:437–47.

894 98. Choudoir MJ, DeAngelis KM. A framework for integrating microbial dispersal modes into
895 soil ecosystem ecology. iScience. 2022;25:103887.

896 99. Emerson JB, Roux S, Brum JR, Bolduc B, Woodcroft BJ, Jang HB, et al. Host-linked soil
897 viral ecology along a permafrost thaw gradient. Nat Microbiol. 2018;3:870–80.

898 100. Narr A, Nawaz A, Wick LY, Harms H, Chatzinotas A. Soil viral communities vary
899 temporally and along a land use transect as revealed by virus-like particle counting and a
900 modified community fingerprinting approach (fRAPD). Front Microbiol. 2017;8:1975.

901 101. Liang X, Wagner RE, Zhuang J, DeBruyn JM, Wilhelm SW, Liu F, et al. Viral abundance
902 and diversity vary with depth in a southeastern united states agricultural ultisol. Soil Biol
903 Biochem. 2019;137:107546.

904 102. Sasidharan S, Torkzaban S, Bradford SA, Kookana R, Page D, Cook PG. Transport and
905 retention of bacteria and viruses in biochar-amended sand. Sci Total Environ. 2016;548–
906 549:100–9.

907 103. Kuzyakov Y, Mason-Jones K. Viruses in soil: nano-scale undead drivers of microbial life,
908 biogeochemical turnover and ecosystem functions. Soil Biol Biochem. 2018;127:305–17.

909 104. Dralle DN, Hahm WJ, Rempe DM, Karst NJ, Thompson SE, Dietrich WE. Quantification
910 of the seasonal hillslope water storage that does not drive streamflow: Catchment storage
911 that does not drive streamflow. Hydrol Process. 2018;32:1978–92.

912 105. Bull J, Christensen K, Scott C, Jack B, Crandall C, Krone S. Phage-bacterial dynamics
913 with spatial structure: self organization around phage sinks can promote increased cell
914 densities. Antibiotics. 2018;7:8.

915 106. Chevallereau A, Pons BJ, van Houte S, Westra ER. Interactions between bacterial and
916 phage communities in natural environments. Nat Rev Microbiol. 2022;20:49–62.

917 107. Simmons M, Drescher K, Nadell CD, Bucci V. Phage mobility is a core determinant of
918 phage–bacteria coexistence in biofilms. ISME J. 2018;12:531–43.

919 108. Starr EP, Nuccio EE, Pett-Ridge J, Banfield JF, Firestone MK. Metatranscriptomic
920 reconstruction reveals RNA viruses with the potential to shape carbon cycling in soil. Proc
921 Natl Acad Sci. 2019;116:25900–8.

922 109. Bondy-Denomy J, Qian J, Westra ER, Buckling A, Guttman DS, Davidson AR, et al.
923 Prophages mediate defense against phage infection through diverse mechanisms. ISME J.
924 2016;10:2854–66.

925 110. Mavrich TN, Hatfull GF. Evolution of superinfection immunity in cluster a
926 mycobacteriophages. mBio. 2019;10:e00971-19.

927 111. Dedrick RM, Jacobs-Sera D, Bustamante CAG, Garlena RA, Mavrich TN, Pope WH, et
928 al. Prophage-mediated defence against viral attack and viral counter-defence. Nat
929 Microbiol. 2017;2:16251.

930 112. Grodzicker T, Arditti RR, Eisen H. Establishment of repression by lambdoid phage in
931 catabolite activator protein and adenylate cyclase mutants of *Escherichia coli*. Proc Natl
932 Acad Sci. 1972;69:366–70.

933 113. Cheng HH, Muhlrad PJ, Hoyt MA, Echols H. Cleavage of the cII protein of phage lambda
934 by purified HflA protease: control of the switch between lysis and lysogeny. Proc Natl Acad
935 Sci. 1988;85:7882–6.

936 114. Silveira CB, Luque A, Rohwer F. The landscape of lysogeny across microbial community
937 density, diversity and energetics. Environ Microbiol. 2021;23:4098–111.

938 115. Mizuno CM, Ghai R, Saghaï A, López-García P, Rodriguez-Valera F. Genomes of
939 abundant and widespread viruses from the deep ocean. mBio. 2016;7:e00805-16.

940 116. Luo E, Aylward FO, Mende DR, DeLong EF. Bacteriophage distributions and temporal
941 variability in the ocean's interior. mBio. 2017;8:e01903-17.

942 117. Coutinho FH, Rosselli R, Rodríguez-Valera F. Trends of microdiversity reveal depth-
943 dependent evolutionary strategies of viruses in the Mediterranean. mSystems.
944 2019;4:e00554-19.

945 118. Li G, Cortez MH, Dushoff J, Weitz JS. When to be temperate: on the fitness benefits of
946 lysis vs. lysogeny. Virus Evol. 2020;6:veaa042.

947 119. Erez Z, Steinberger-Levy I, Shamir M, Doron S, Stokar-Avihail A, Peleg Y, et al.
948 Communication between viruses guides lysis–lysogeny decisions. Nature. 2017;541:488–
949 93.

950 120. Shkoporov AN, Khokhlova EV, Fitzgerald CB, Stockdale SR, Draper LA, Ross RP, et al.
951 ΦCrAss001 represents the most abundant bacteriophage family in the human gut and infects
952 Bacteroides intestinalis. Nat Commun. 2018;9:4781.

953 121. Iyer LM, Anantharaman V, Krishnan A, Burroughs MA, Aravind L. Jumbo phages: a
954 comparative genomic overview of core functions and adaptions for biological conflicts.
955 Viruses. 2021;13:63.

956 122. Weinheimer AR, Aylward FO. Infection strategy and biogeography distinguish
957 cosmopolitan groups of marine jumbo bacteriophages. ISME J. 2022;16:1657–67.

958 123. Hua J, Huet A, Lopez CA, Toropova K, Pope WH, Duda RL, et al. Capsids and Genomes
959 of Jumbo-Sized Bacteriophages Reveal the Evolutionary Reach of the HK97 Fold. mBio.
960 2017;8:e01579-17.

961 124. Schulz F, Alteio L, Goudeau D, Ryan EM, Yu FB, Malmstrom RR, et al. Hidden diversity
962 of soil giant viruses. Nat Commun. 2018;9:4881.

963 125. Jin M, Guo X, Zhang R, Qu W, Gao B, Zeng R. Diversities and potential biogeochemical
964 impacts of mangrove soil viruses. Microbiome. 2019;7:58.

965 126. Hill P, Krištůfek V, Dijkhuizen L, Boddy C, Kroetsch D, van Elsas JD. Land use intensity
966 controls actinobacterial community structure. Microb Ecol. 2011;61:286–302.

967 127. Eisenlord SD, Zak DR. Simulated atmospheric nitrogen deposition alters actinobacterial
968 community composition in forest soils. Soil Sci Soc Am J. 2010;74:1157–66.

969 128. Santos-Medellín C, Liechty Z, Edwards J, Nguyen B, Huang B, Weimer BC, et al.
970 Prolonged drought imparts lasting compositional changes to the rice root microbiome. Nat
971 Plants. 2021;7:1065–77.

972 129. Van Goethem MW, Swenson TL, Trubl G, Roux S, Northen TR. Characteristics of
973 wetting-induced bacteriophage blooms in biological soil crust. mBio. 2019;10:e02287-19,
974 /mbio/10/6/mBio.02287-19.atom.

975 130. Barnard RL, Osborne CA, Firestone MK. Responses of soil bacterial and fungal
976 communities to extreme desiccation and rewetting. ISME J. 2013;7:2229–41.

977 131. Dion MB, Oechslin F, Moineau S. Phage diversity, genomics and phylogeny. Nat Rev
978 Microbiol. 2020;18:125–38.

979 132. Hughes AR, Inouye BD, Johnson MTJ, Underwood N, Vellend M. Ecological
980 consequences of genetic diversity. Ecol Lett. 2008;11:609–23.

981 133. Larkin AA, Martiny AC. Microdiversity shapes the traits, niche space, and biogeography
982 of microbial taxa. Environ Microbiol Rep. 2017;9:55–70.

983 134. Brown BP, Wendoh J, Chopera D, Havyarimana E, Jaumdally S, Nyangahu DD, et al.
984 crAssphage abundance and genomic selective pressure correlate with altered bacterial
985 abundance in the fecal microbiota of South African mother-infant dyads. preprint.
986 Microbiology; 2019.

987 135. Siranosian BA, Tamburini FB, Sherlock G, Bhatt AS. Acquisition, transmission and strain
988 diversity of human gut-colonizing crAss-like phages. Nat Commun. 2020;11:280.

989 136. Zhao F, Lin X, Cai K, Jiang Y, Ni T, Chen Y, et al. Integration of the cyanophage-encoded
990 phosphate binding protein into the cyanobacterial phosphate uptake system. preprint.
991 Microbiology; 2021.

992 137. Bernheim A, Sorek R. The pan-immune system of bacteria: antiviral defence as a
993 community resource. Nat Rev Microbiol. 2020;18:113–9.

994 138. Makarova KS, Wolf YI, Snir S, Koonin EV. Defense islands in bacterial and archaeal
995 genomes and prediction of novel defense systems. J Bacteriol. 2011;193:6039–56.

996 139. Broniewski JM, Meaden S, Paterson S, Buckling A, Westra ER. The effect of phage
997 genetic diversity on bacterial resistance evolution. ISME J. 2020;14:828–36.

998

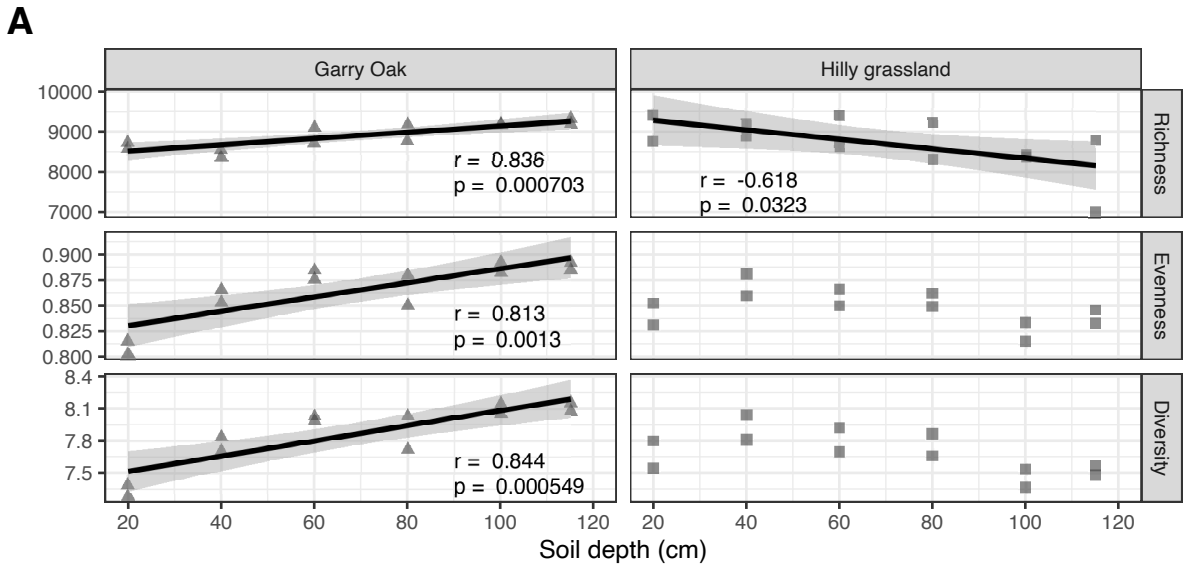

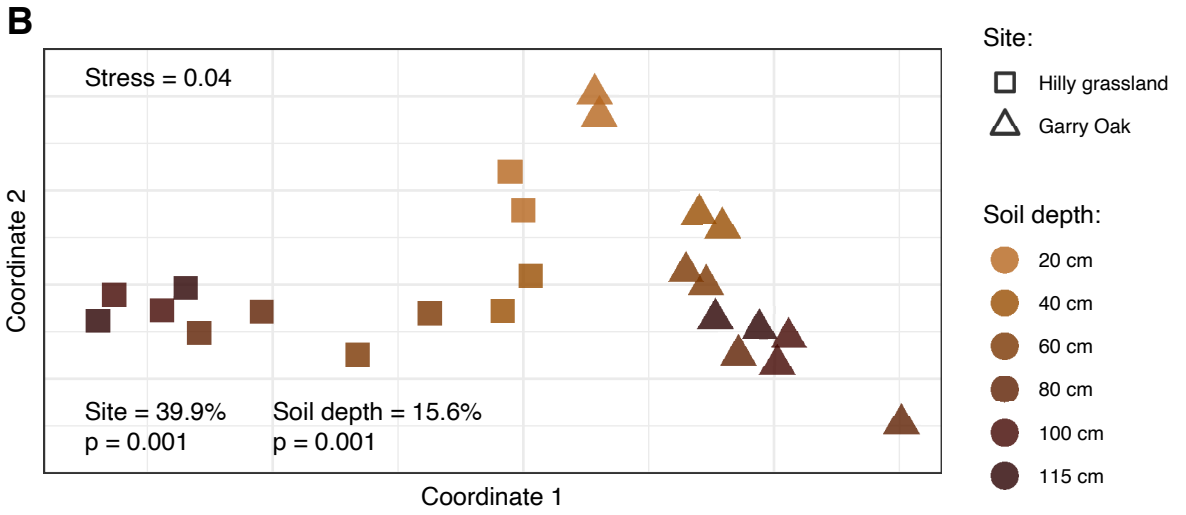

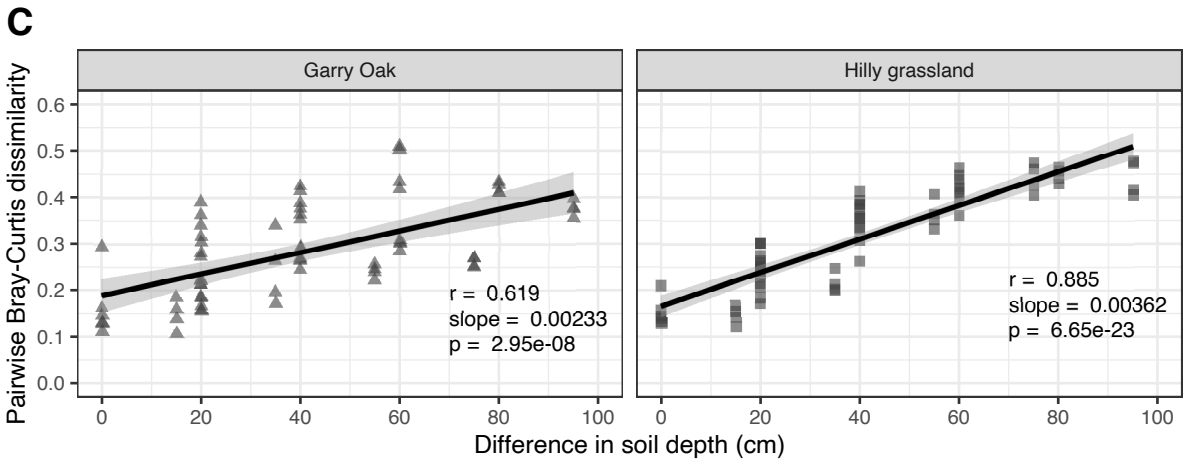

999

Fig. 1: Population-level assembly of soil viral communities throughout soil depth. A Alpha diversity of viral communities. Richness (number of vOTUs detected), evenness (Pielou's J index), and alpha diversity (Shannon's H index) for each viral community throughout the soil depth profiles. Trend lines represent linear regression estimates, with shaded cloud representing 95% confidence interval. r corresponds to Pearson's correlation coefficient and p corresponds to the associated p-value. **B** Beta diversity of viral communities. Non-metric multidimensional scaling (NMDS) ordination plots, representing the Bray-Curtis dissimilarities between viral community compositions. Shapes indicate site: Hilly grassland (squares) and Garry Oak (triangles). Shapes are coloured based on soil depth. Stress value associated with two-dimensional ordination is reported. Percentage contribution to variance by site and soil depth, as calculated with a permutational multivariate analysis of variance (PERMANOVA) test, and associated p-value are also reported. **C** Distance-decay relationship in viral community structure. Trend lines represent linear regression estimates, with shaded cloud representing 95% confidence interval. r corresponds to Pearson's correlation coefficient, slope corresponds to linear regression slope, and p corresponds to the associated p-value.

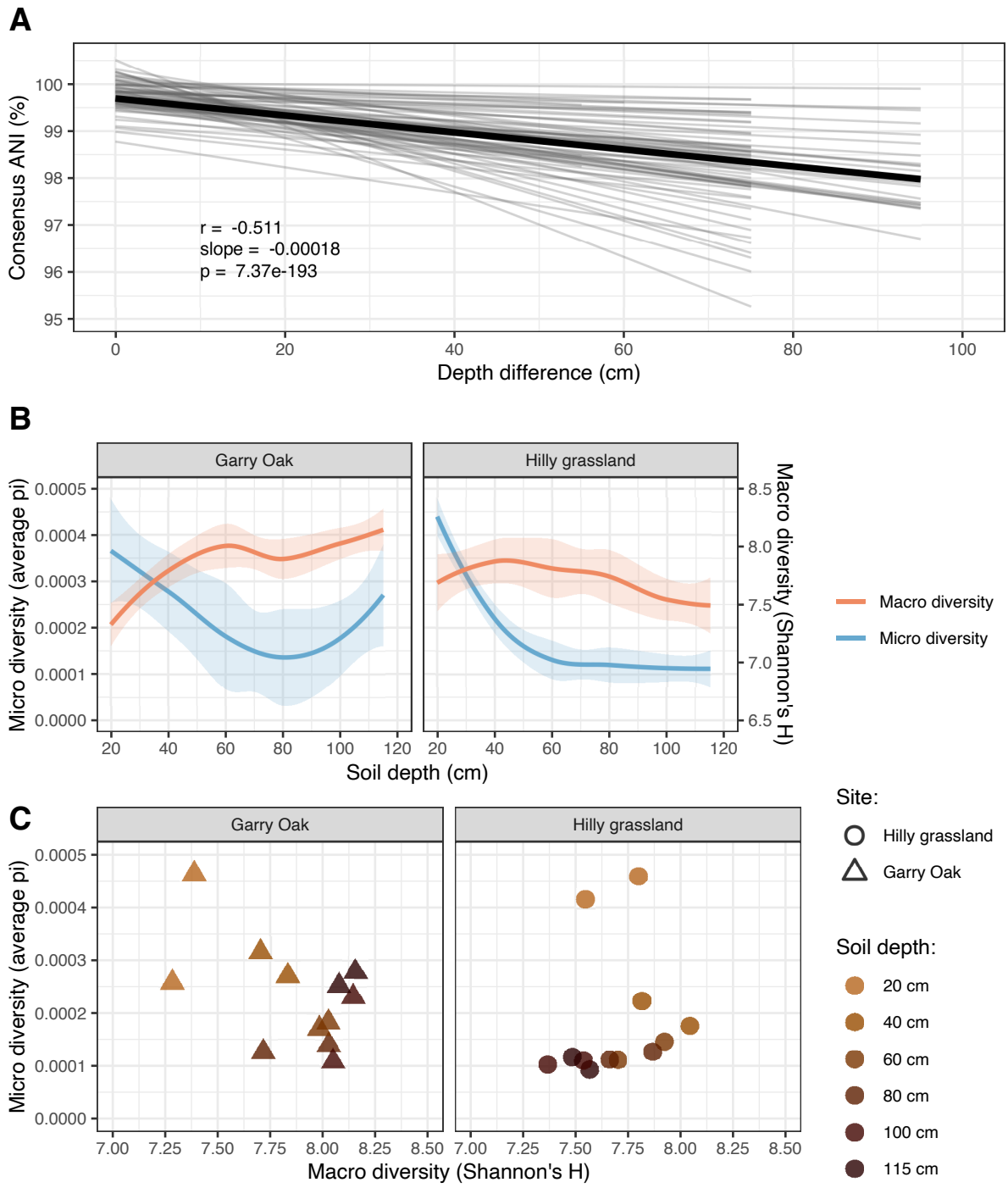

1016
1017

Fig. 2: Strain-level assembly of soil viral communities throughout soil depth. A Distance decay relationship in consensus ANI. Lighter grey lines represent distance-decay relationships in consensus ANI for 69 vOTUs with individual significant relationships. Thicker black line represents the mean distance decay relationship across all 69 vOTUs. Trend lines represent linear regression estimates, with shaded cloud representing 95% confidence interval. r corresponds to Pearson's correlation coefficient, slope corresponds to linear regression slope, and p corresponds to the associated p-value. **B** Viral macro diversity and micro diversity throughout the soil depth profiles. Trend lines represent loess smooth regression estimates, with shaded cloud representing 95% confidence interval. Colour indicates level of diversity: macro diversity (red), micro diversity (blue). **C** Correlation of macro diversity with micro diversity. Shapes indicate site: Hilly grassland (squares) and Garry Oak (triangles). Shapes are coloured based on soil depth.

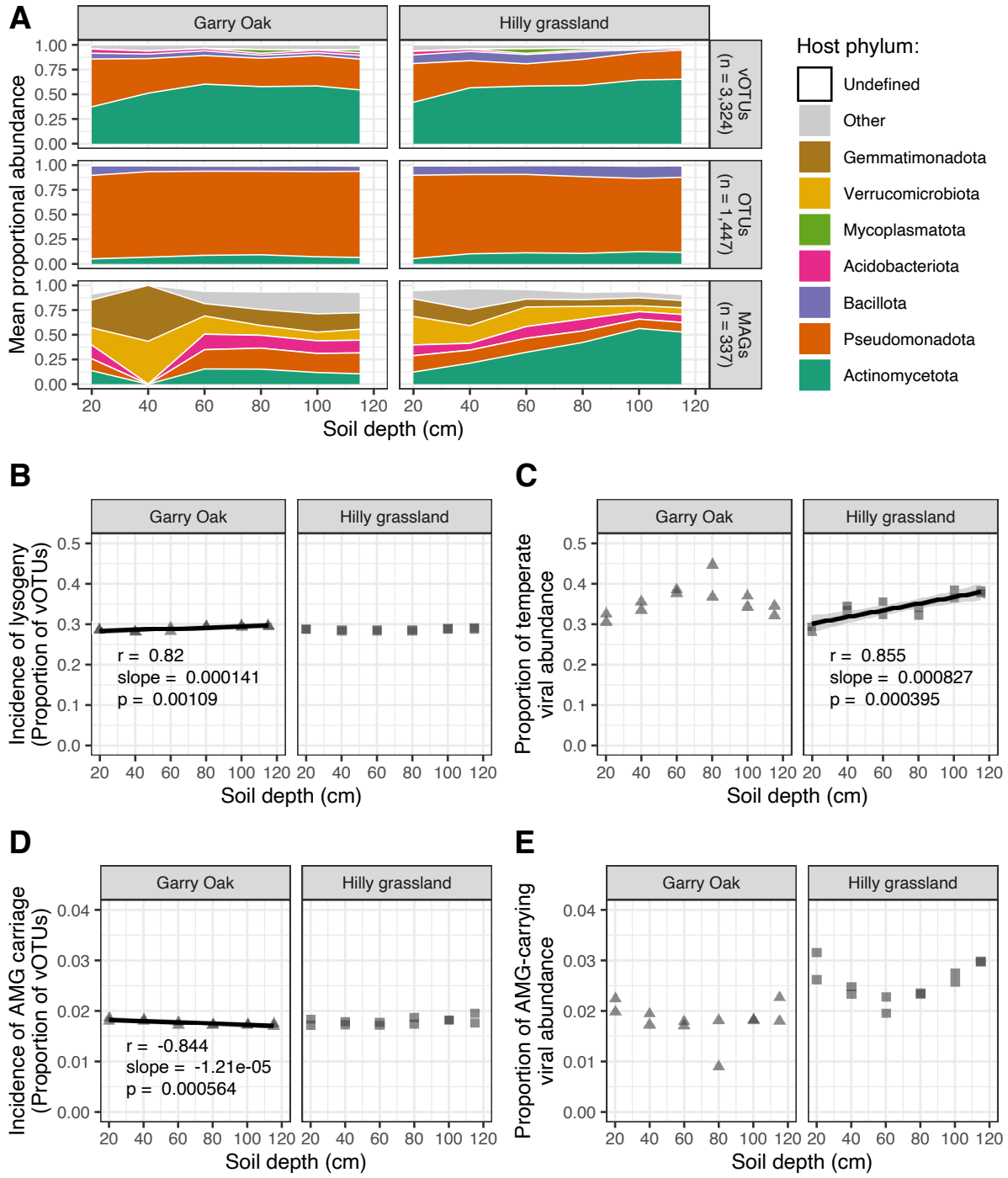

1031

Fig. 3: Virus-host interactions throughout soil depth. A Virus-host linkages. Mean proportional abundance by host phyla is plotted across soil depth for: vOTUs with predicted host phyla (n = 3324), microbial OTUs (n = 1447), and microbial MAGs (n = 337). Fill colour indicates host phylum. **B** Incidence of lysogeny. Proportion of vOTUs detected representing temperate viruses plotted across soil depth. **C** Temperate viral abundance. Proportional abundance of vOTUs detected representing temperate viruses plotted across soil depth. **D** Incidence of AMG carriage. Proportion of vOTUs carrying AMGs plotted across soil depth. **E** AMG-carrying viral abundance. Proportional abundance of vOTUs carrying AMGs plotted across soil depth. For **B**, **C**, and **D**, trend lines represent linear regression estimates, with shaded cloud representing 95% confidence interval. r corresponds to Pearson's correlation coefficient, slope corresponds to linear regression slope, and p corresponds to the associated p-value.

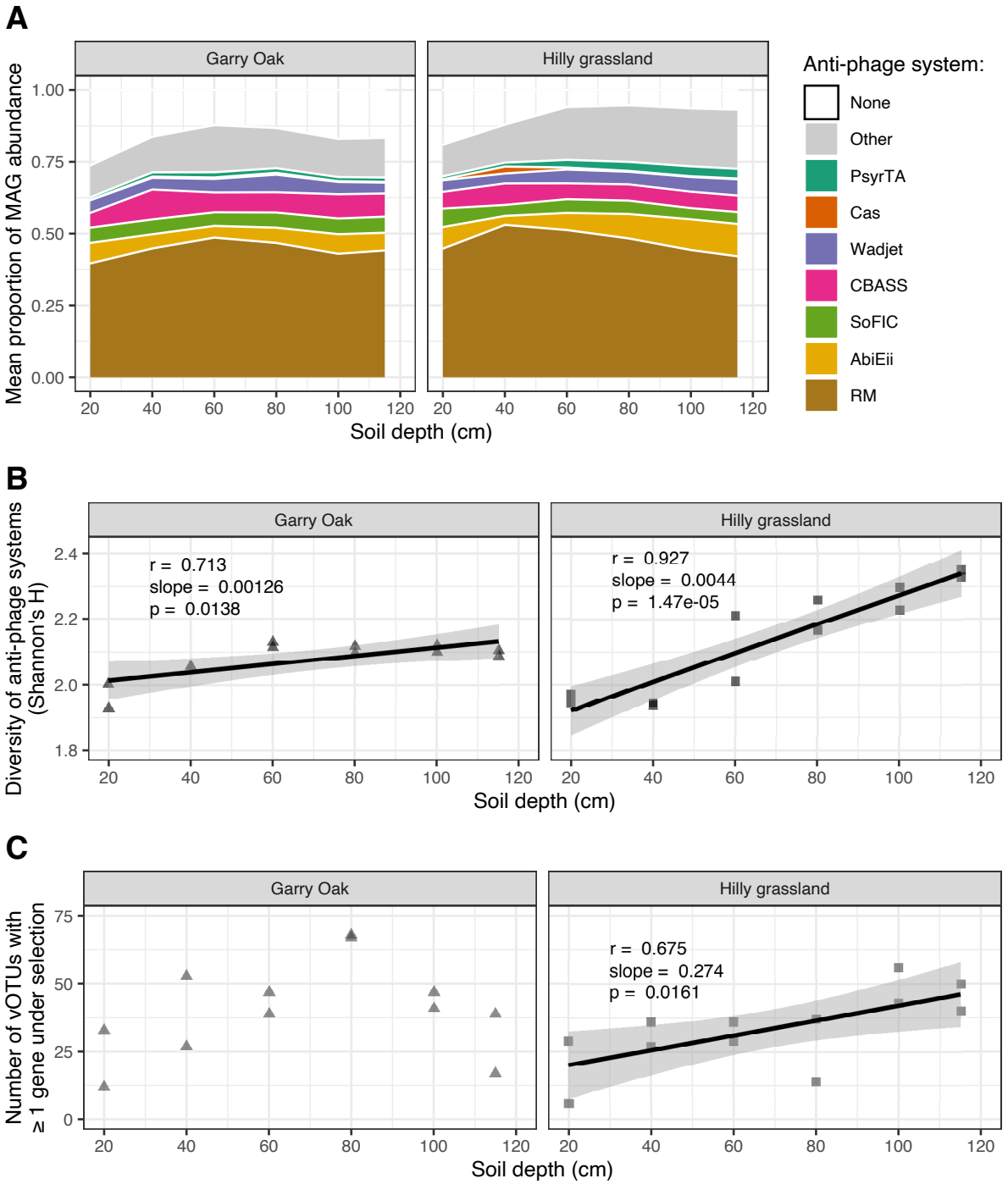

1044

Fig. 4: Virus-host antagonistic co-evolution throughout soil depth. A Anti-phage system detection. Proportional abundance of microbial MAGs carrying complete anti-phage systems. Fill colour indicates anti-phage system. **B** Diversity of the anti-phage system repertoire. Shannon's H index, calculated on MAGs carrying complete anti-phage systems, plotted across soil depth. **C** Viruses under positive selection. Number of vOTU genomes with at least one gene under positive selection (indicated by a pN/pS ratio > 1) plotted across soil depth. For **B** and **C**, trend lines represent linear regression estimates, with shaded cloud representing 95% confidence interval. r corresponds to Pearson's correlation coefficient, slope corresponds to linear regression slope, and p corresponds to the associated p-value.

1055

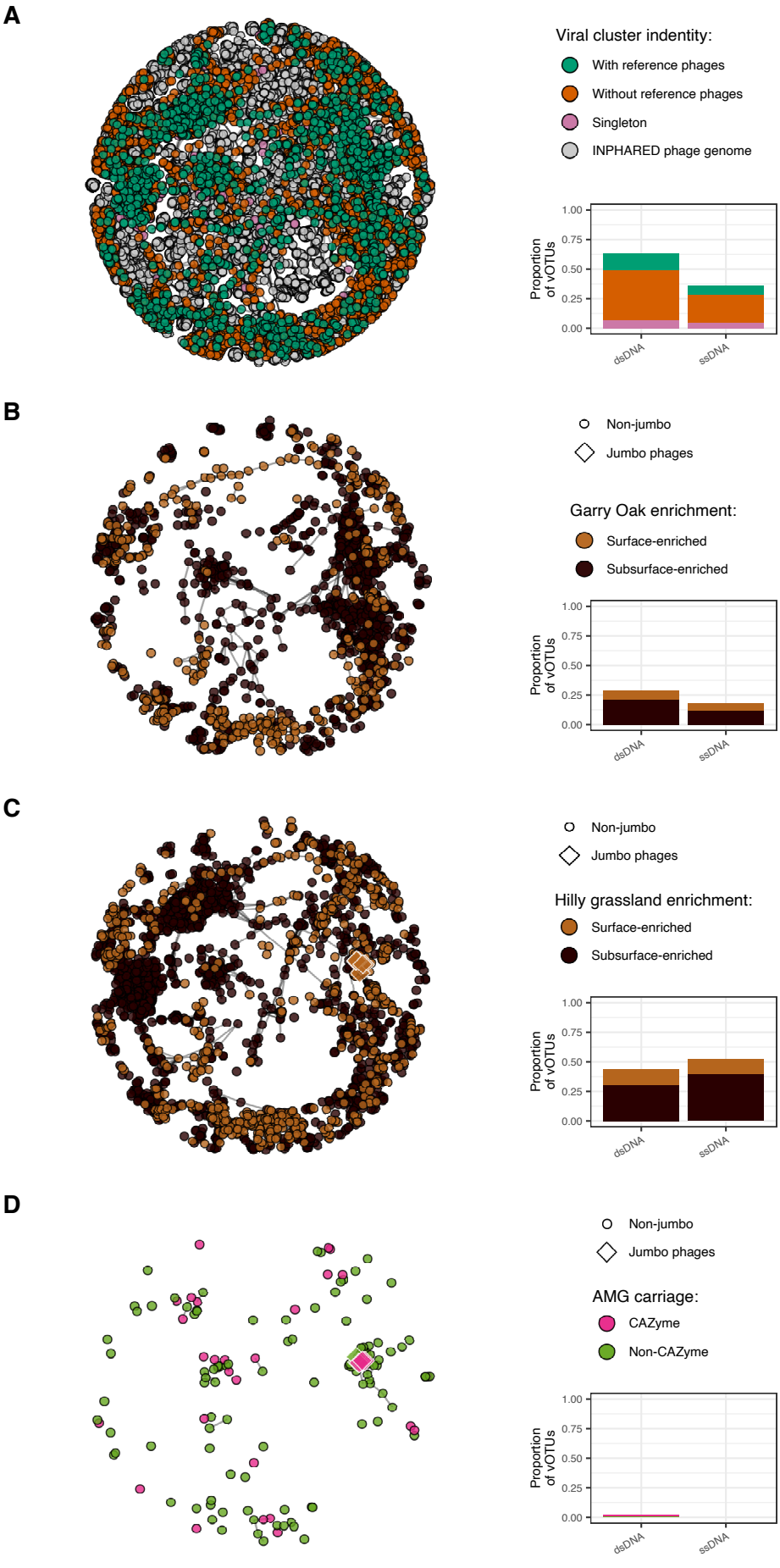

Fig. S1: Taxonomic novelty of recovered soil vOTUs. Shared protein content of recovered soil vOTUs with previously discovered phage genomes. Network graph visualisations are annotated to represent **A** viral cluster identities (6124 dsDNA vOTUs, 193 ssRNA vOTUs, and 11,600 reference genomes), **B** depth enrichment in Garry Oak (1637 dsDNA vOTUs, 19 ssDNA vOTUs), **C** depth enrichment in Hilly grassland (2820 dsDNA vOTUs, 138 ssDNA vOTUs), and **D** vOTUs carrying AMGs (152 dsDNA vOTUs, 0 ssDNA vOTUs). Bar charts (right) summarise the proportion of dsDNA vOTUs and ssDNA vOTUs included in each network visualisation. Depth enrichment represents vOTUs enriched in either surface soil (20 cm) or subsurface soil (40 cm – 115 cm).

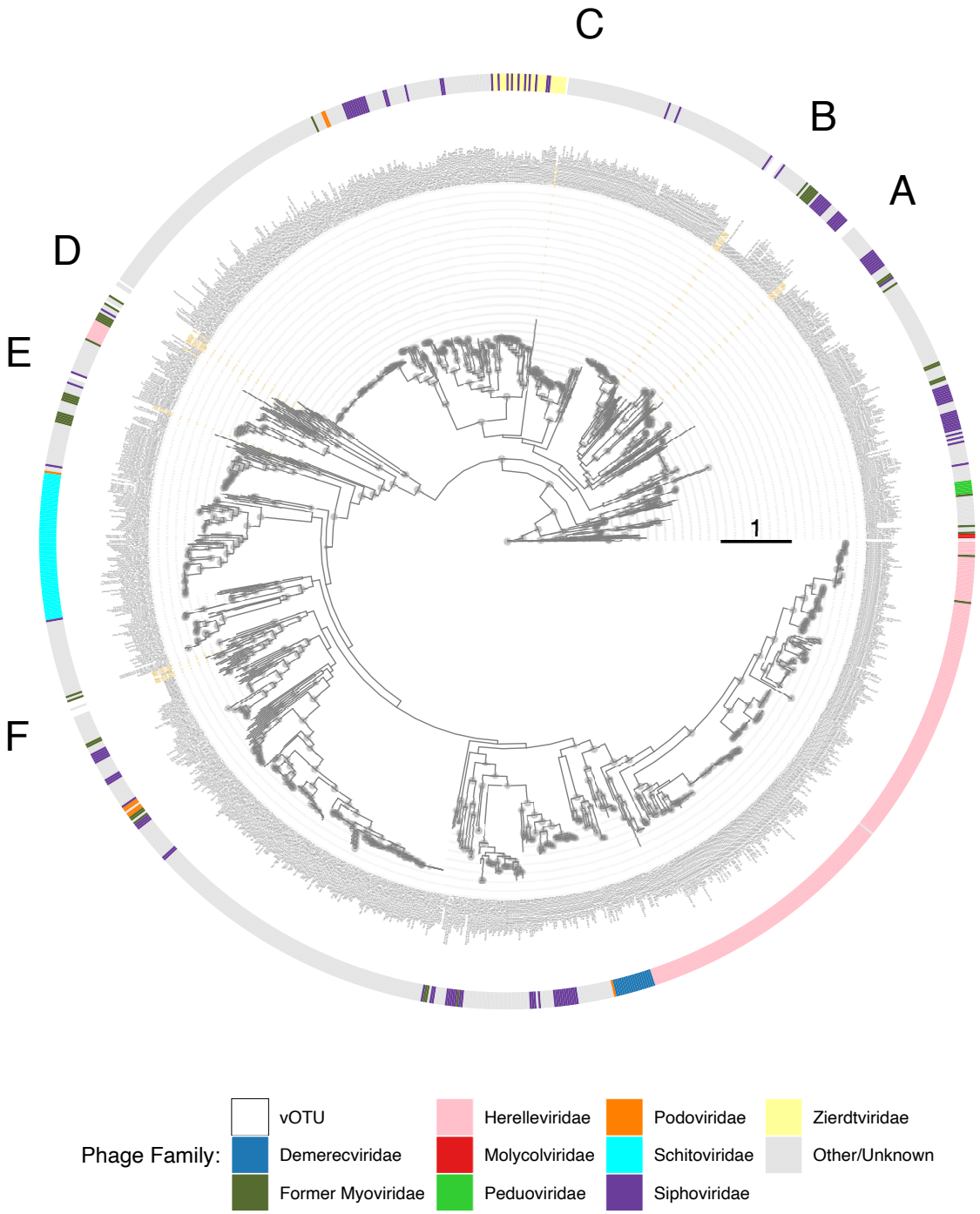

1066

Fig. S2: Phylogenetic assessment of jumbo phage vOTUs and jumbo-related vOTUs using DNA polymerase gene. Phylogeny of jumbo phage vOTUs and vOTUs sharing viral clusters with jumbo phage vOTUs (jumbo-related vOTUs) using translated DNA polymerase sequences. Phylogenetic tree contains 1284 DNA polymerase sequences from 1205 previously isolated phage sequences and 24 DNA polymerase sequences from 14 vOTUs recovered in this study (eight jumbo phage vOTUs and six jumbo-related vOTUs). Brand node labels indicate branch support: ≥ 0.9 (large circles), ≥ 0.8 (medium circles), ≥ 0.7 (small circles), < 0.7 (no circle). Tip labels indicate genome sequence name; vOTUs recovered in this study are labelled in gold. Outer ring fill colour denotes known phage families. Letters indicate the locations of 6 distinct phylogenetic groups of jumbo phage vOTUs and jumbo-related vOTUs.

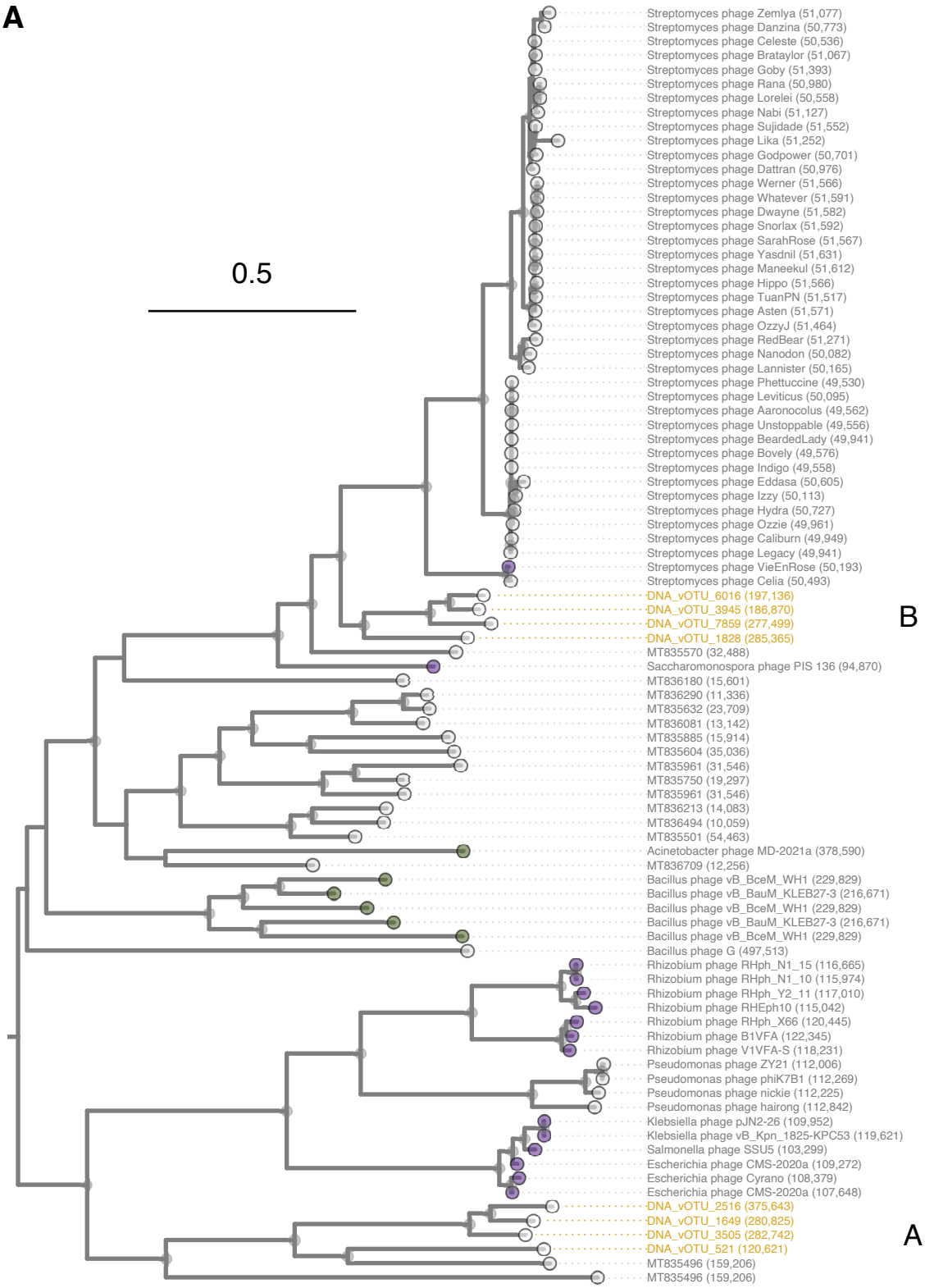

1078

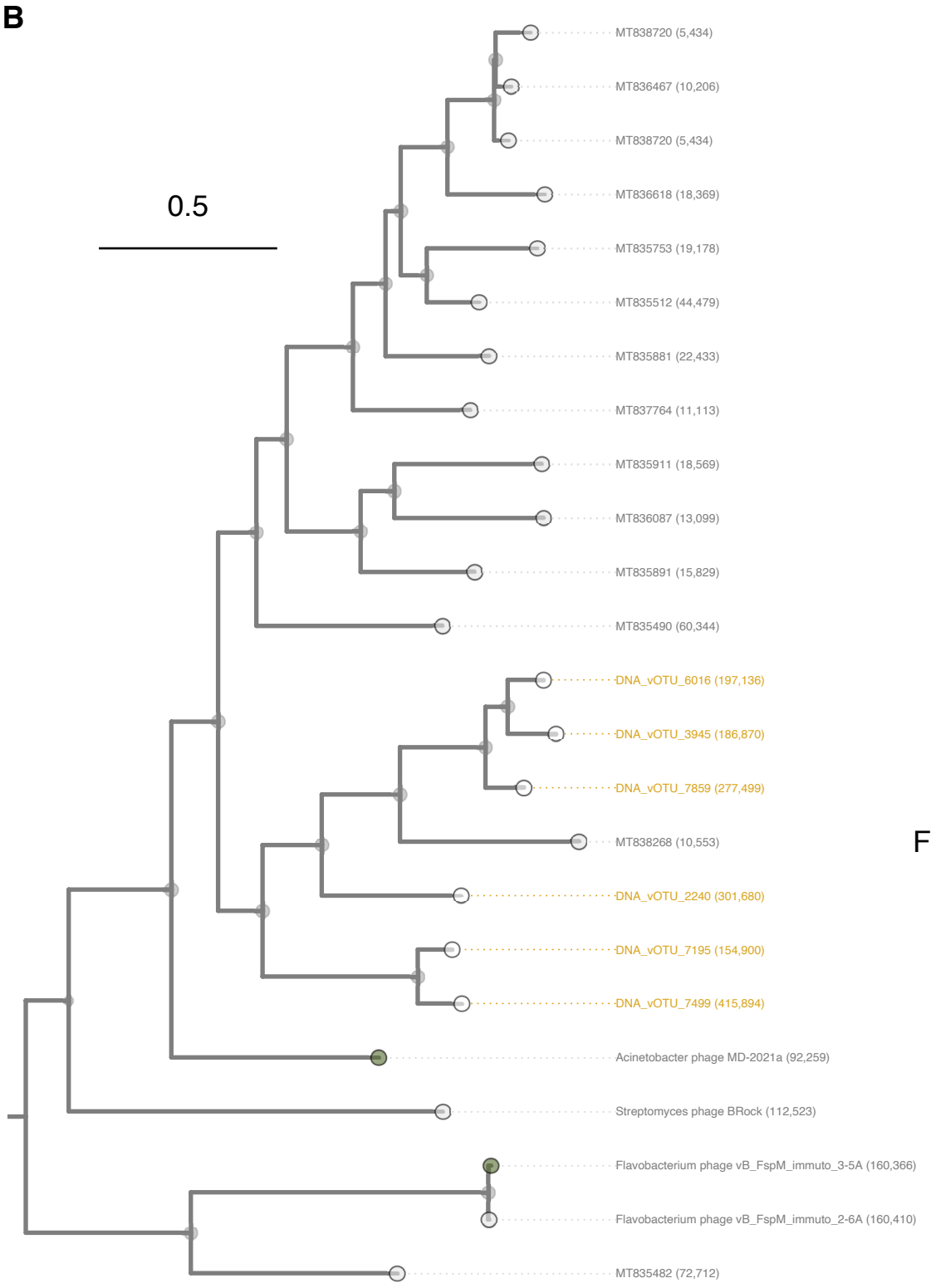

F

1079

Fig. S3: Phylogenetic groups A, B, and F from assessment of jumbo phage vOTUs and jumbo-related vOTUs using DNA polymerase gene. Further investigation of distinct phylogenetic groups identified from Fig. S2: **A** Groups A and B, **B** Group F. Brand node labels indicate branch support: ≥ 0.9 (large circles), ≥ 0.8 (medium circles), ≥ 0.7 (small circles), < 0.7 (no circle). Tip node fill colour denotes known phage families. Tip labels indicate genome sequence name and genome length in bp; vOTUs recovered in this study are labelled in gold. Letters indicate the locations of distinct phylogenetic groups of jumbo phage vOTUs and jumbo-related vOTUs.

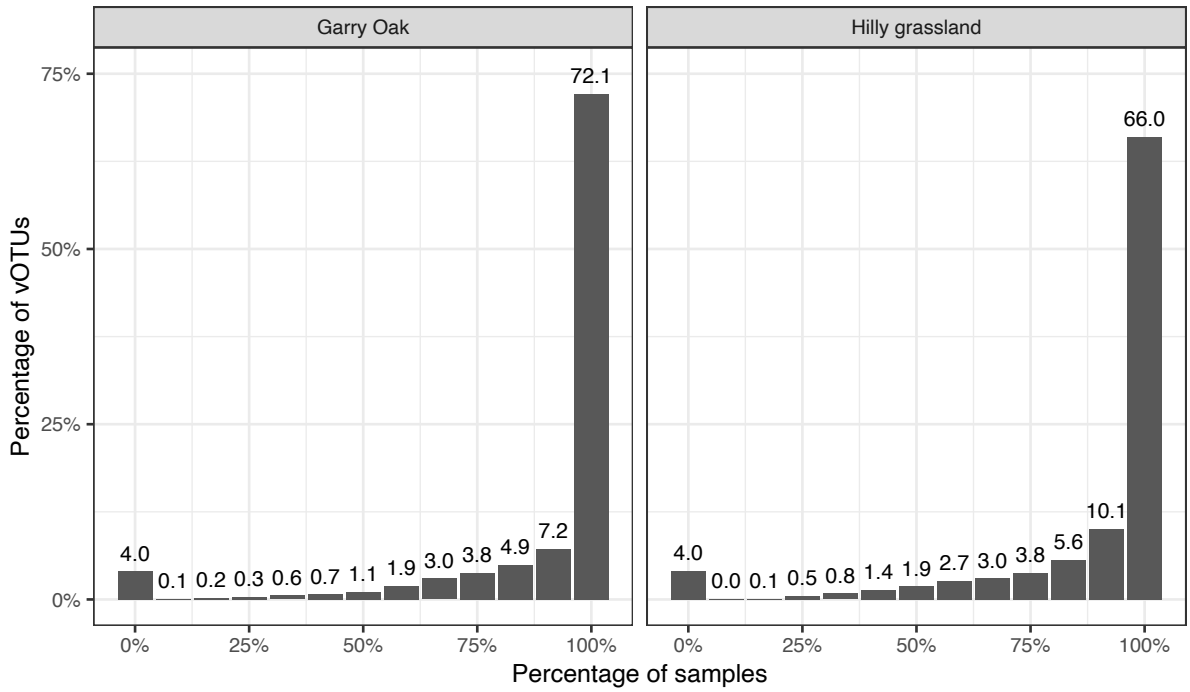

1089

1090 **Fig. S4: Prevalence of viral populations.** Percentage of vOTUs detected in at each percentage

1091 of soil samples. Number above bars specify the percentage of vOTUs detected.

1092

1093

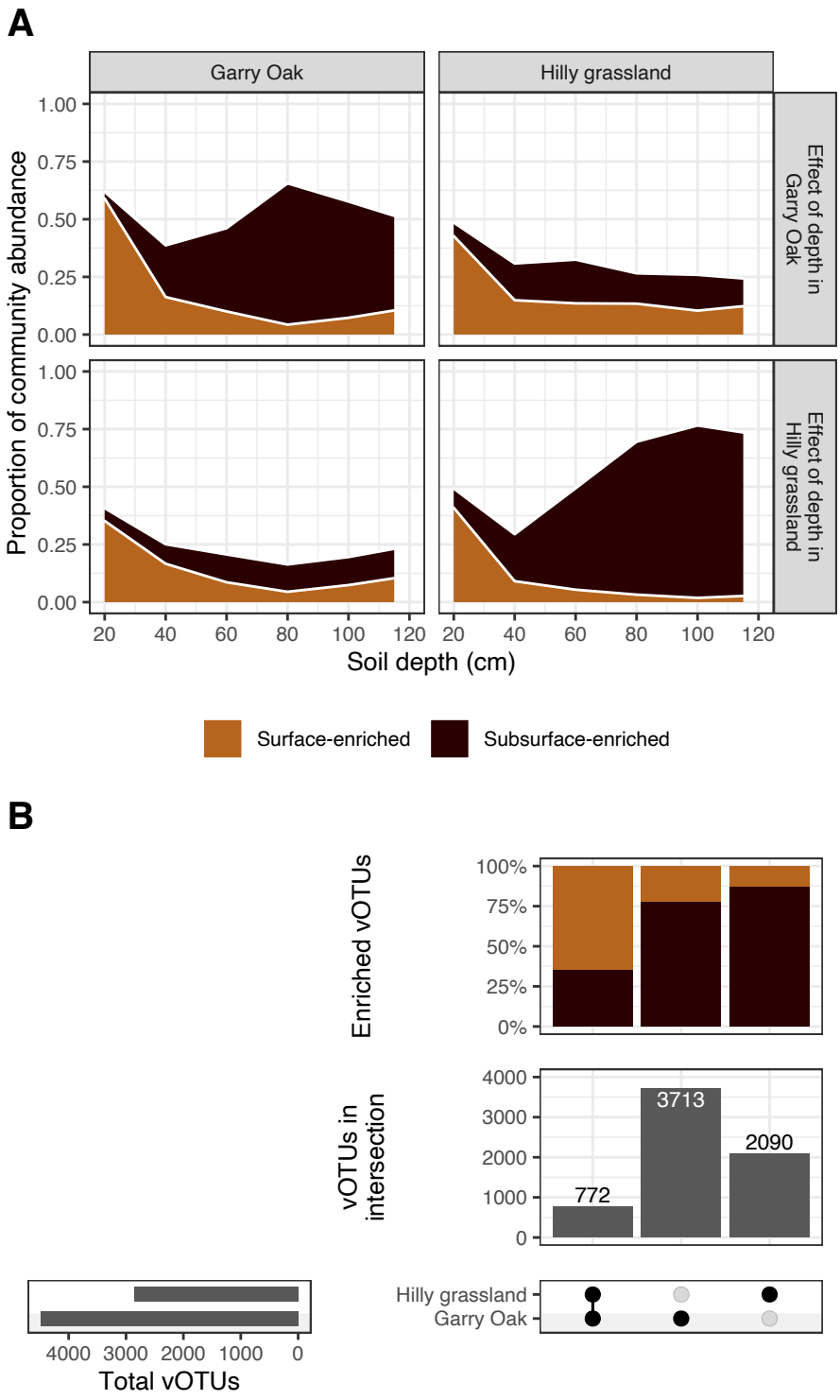

Fig. S5: Overlap in depth-enrichment of viral populations between sites. A Relative abundance of depth-enriched viral populations. Proportional abundance of vOTUs enriched in either surface soil (20 cm) or subsurface soil (40 cm – 115 cm) based on samples derived from Garry Oak and Hilly grassland, across Garry Oak and Hilly grassland samples, respectively. Fill colour indicates enrichment: surface-enriched (light brown) or subsurface enriched (dark brown). **B** Overlap in depth enrichment of viral populations between sites. Intersection matrix denoting site investigated (bottom-right), total vOTUs detected in each site (bottom-left), number of enriched vOTUs in site intersection (middle-right), percentage of enriched vOTUs corresponding to surface-enriched or subsurface-enriched, respectively (top-right).

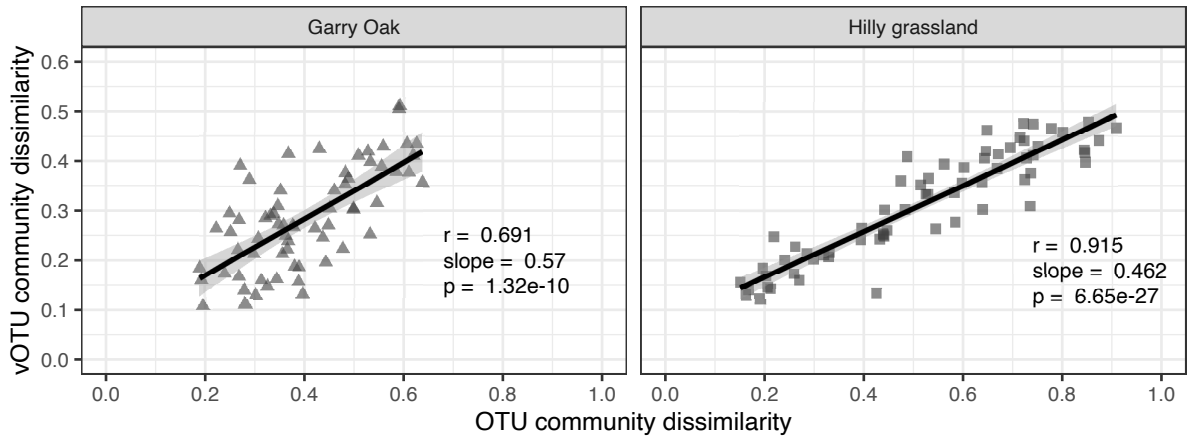

1104

1105 **Fig. S6: Correlation of viral community and microbial community structure.** Trend lines
1106 represent linear regression estimates, with shaded cloud representing 95% confidence interval.
1107 r corresponds to Pearson's correlation coefficient and p corresponds to the associated p-value.
1108

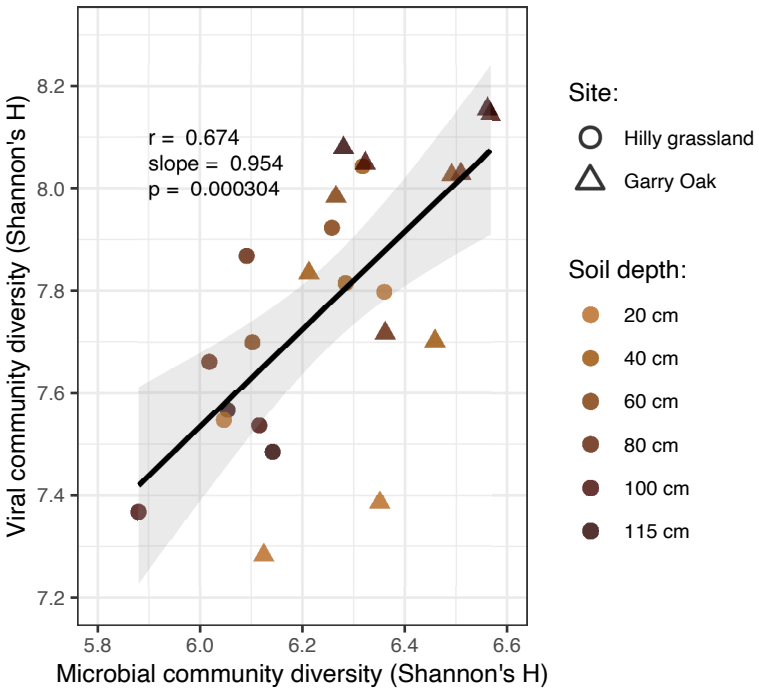

1109

Fig. S7: Correlation of viral community and microbial community diversity. Trend line represents linear regression estimates, with shaded cloud representing 95% confidence interval. r corresponds to Pearson's correlation coefficient and p corresponds to the associated p-value. Shapes indicate site: Hilly grassland (squares) and Garry Oak (triangles). Shapes are coloured based on soil depth.

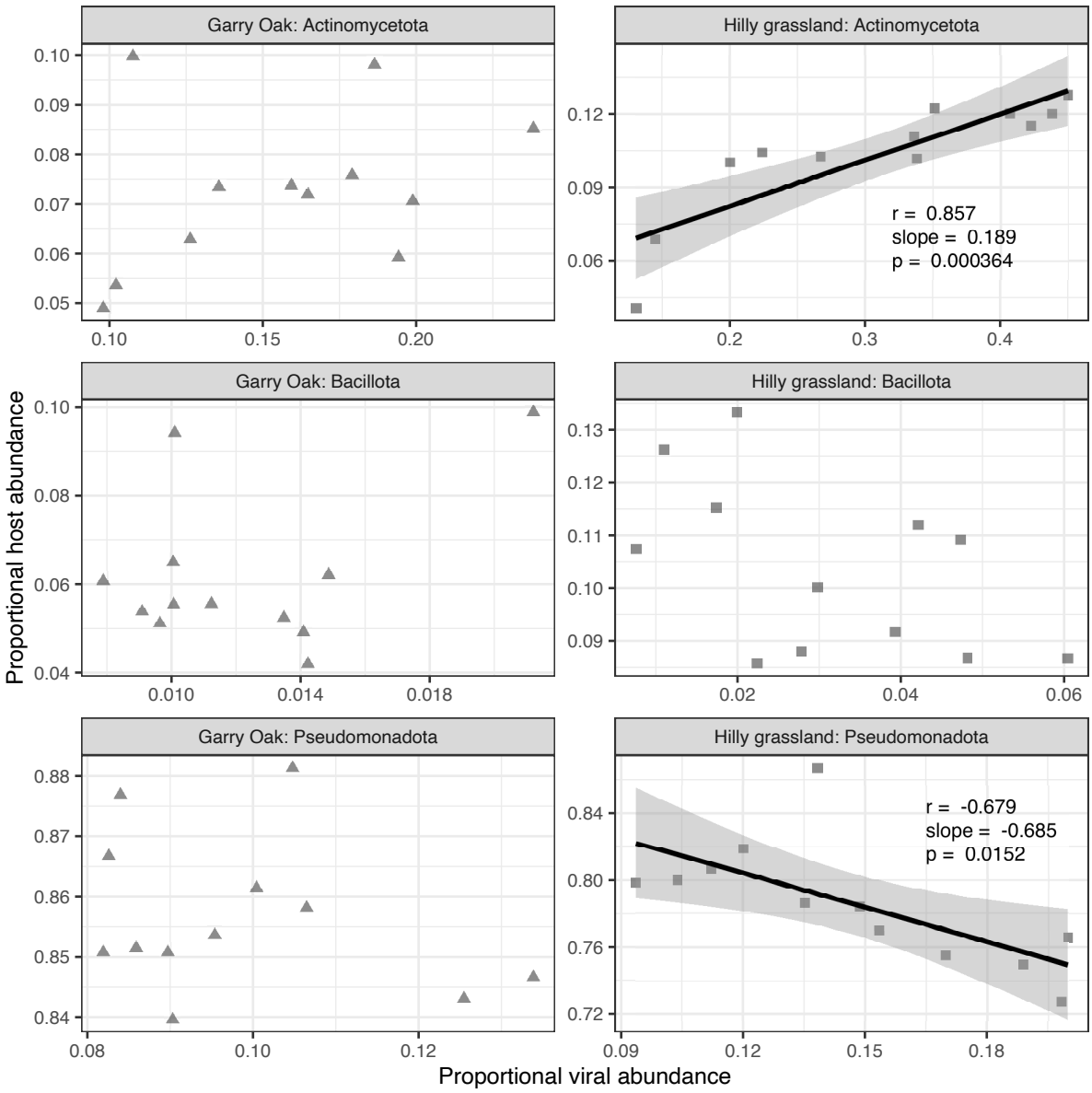

1116

Fig. S8: Correlation of viral abundances and host abundances. Trend line represents linear regression estimates, with shaded cloud representing 95% confidence interval. r corresponds to Pearson's correlation coefficient and p corresponds to the associated p-value.

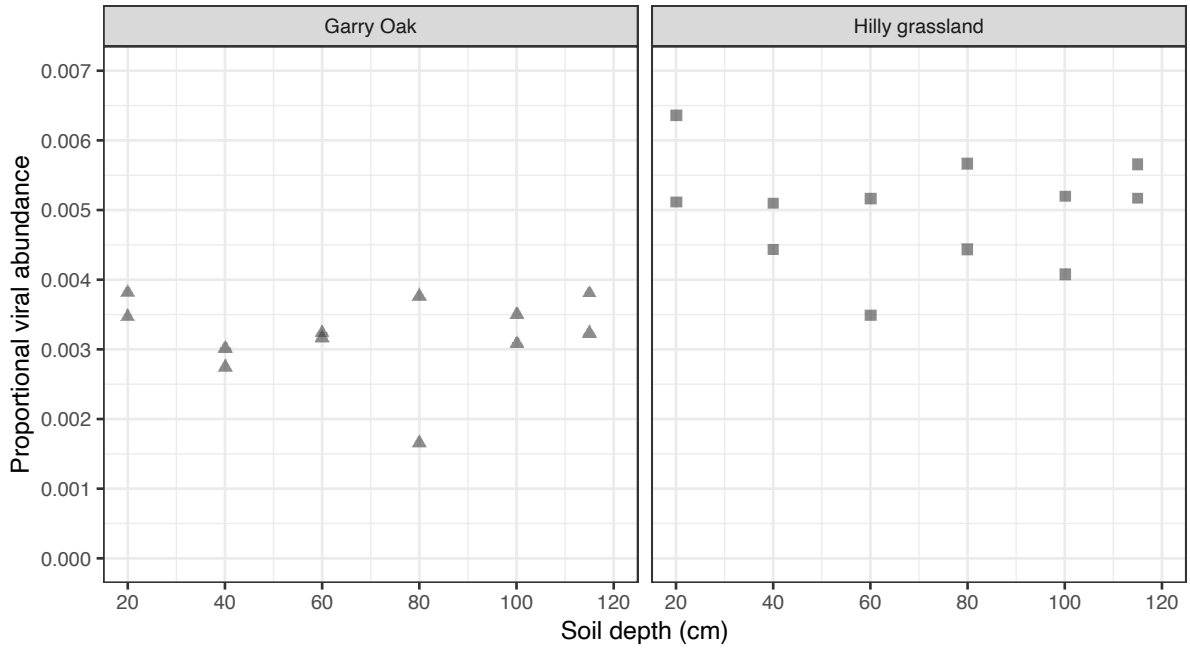

1121

1122 **Fig. S9: Relative abundance of viruses carrying carbohydrate-active enzymes.**

1123

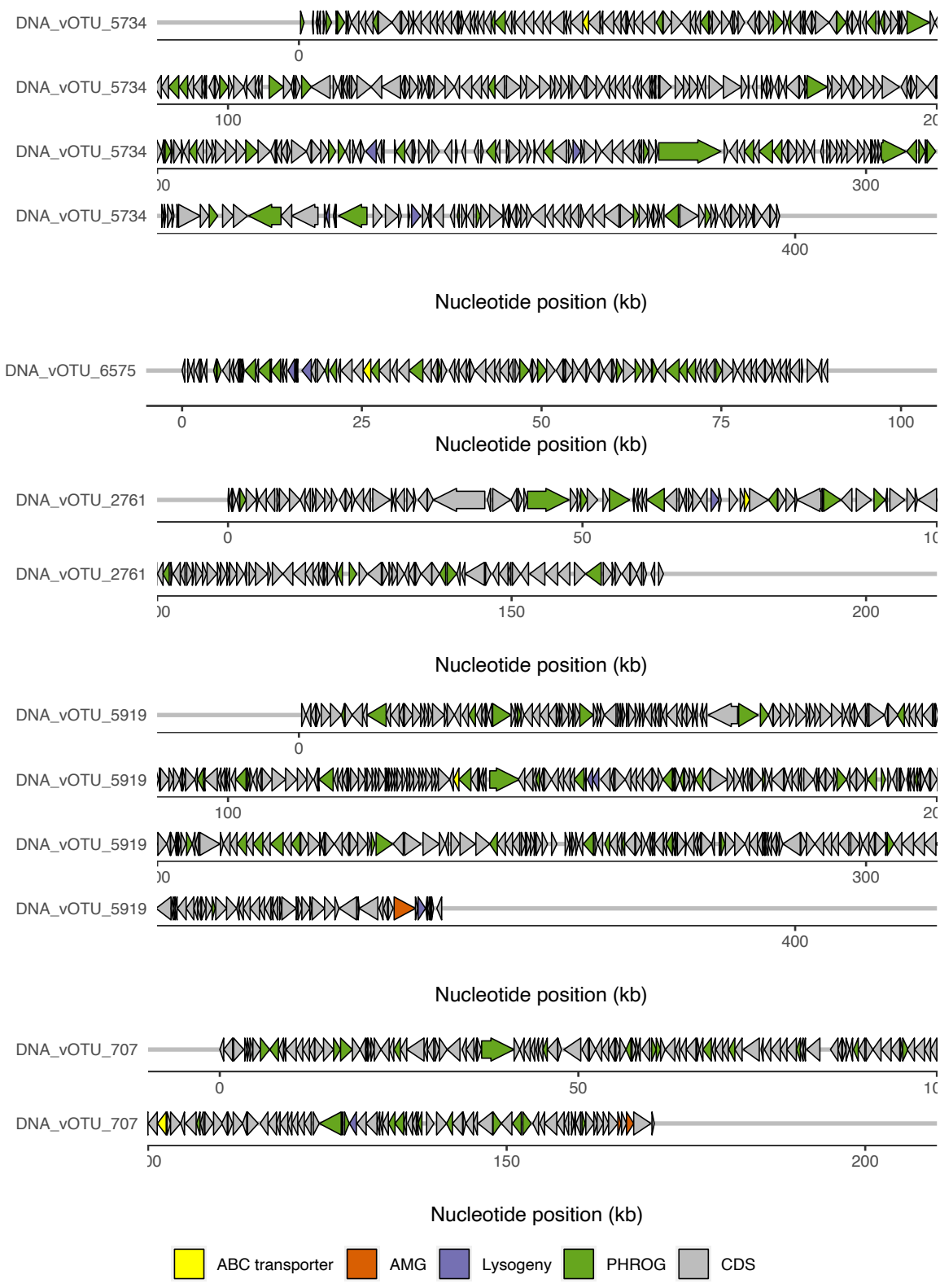

1124

1125 **Fig. S10: Genome maps of high-quality viral genomes carrying ABC transporters under**

1126 **positive selection.** Arrow fill colour indicates gene function.

1127

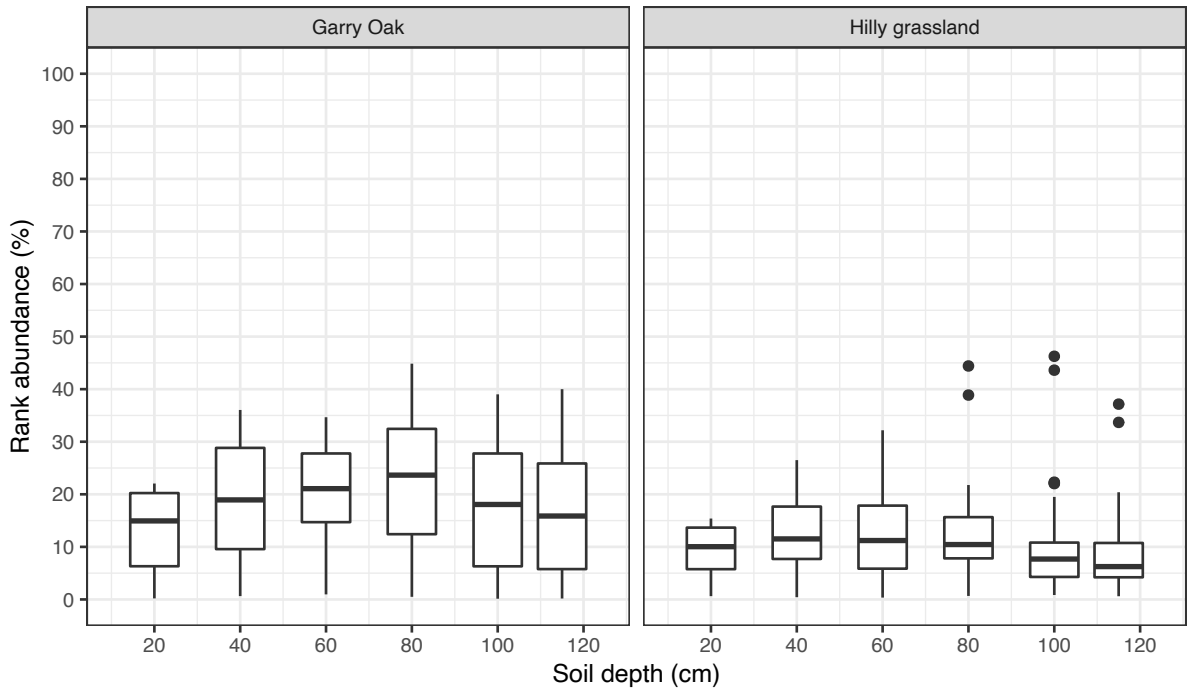

1128

1129 **Fig. S11: Rank abundance of jumbo phages.** Rank abundance represented as a percentage
1130 of 10,196 vOTUs. 0% indicates the lowest rank and the most abundant vOTU, while 100%
1131 indicates the highest rank and the least abundant vOTU. Boxes denote median, upper, and
1132 lower quartiles. Whiskers indicate minimal and maximal values, with outliers in filled circles.
1133

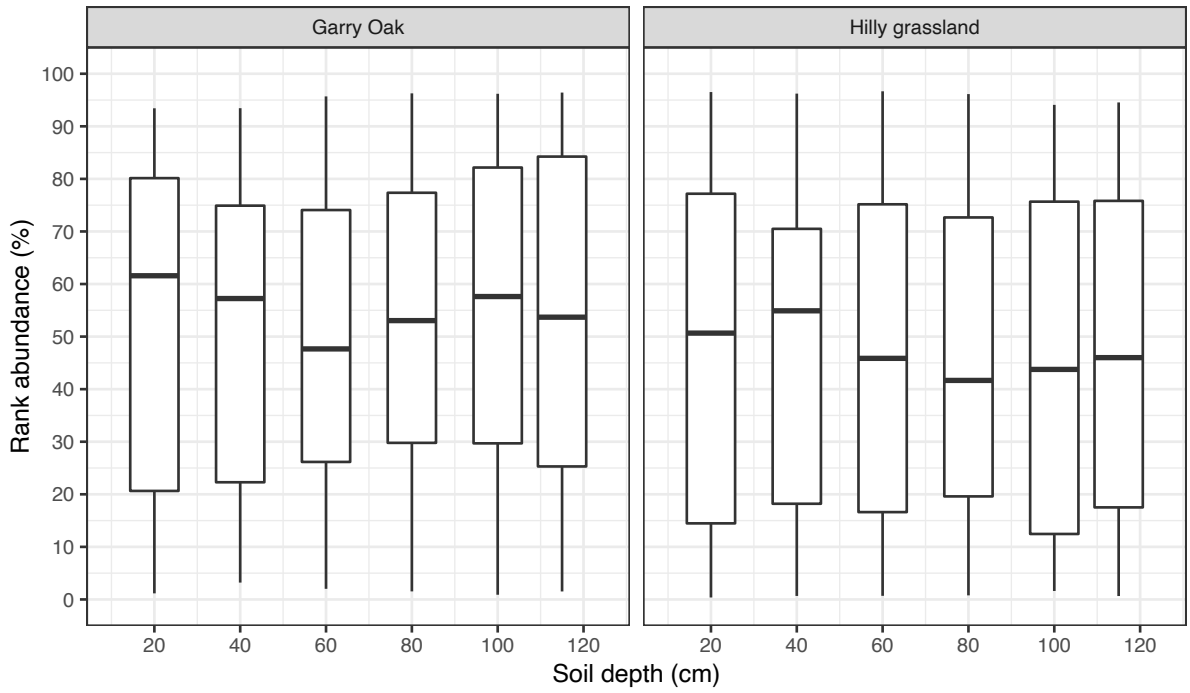

1134

1135 **Fig. S12: Rank abundance of CAZyme-carrying vOTUs.** Rank abundance represented as a
1136 percentage of 10,196 vOTUs. 0% indicates the lowest rank and the most abundant vOTU, while
1137 100% indicates the highest rank and the least abundant vOTU. Boxes denote median, upper,
1138 and lower quartiles. Whiskers indicate minimal and maximal values, with outliers in filled
1139 circles.
1140

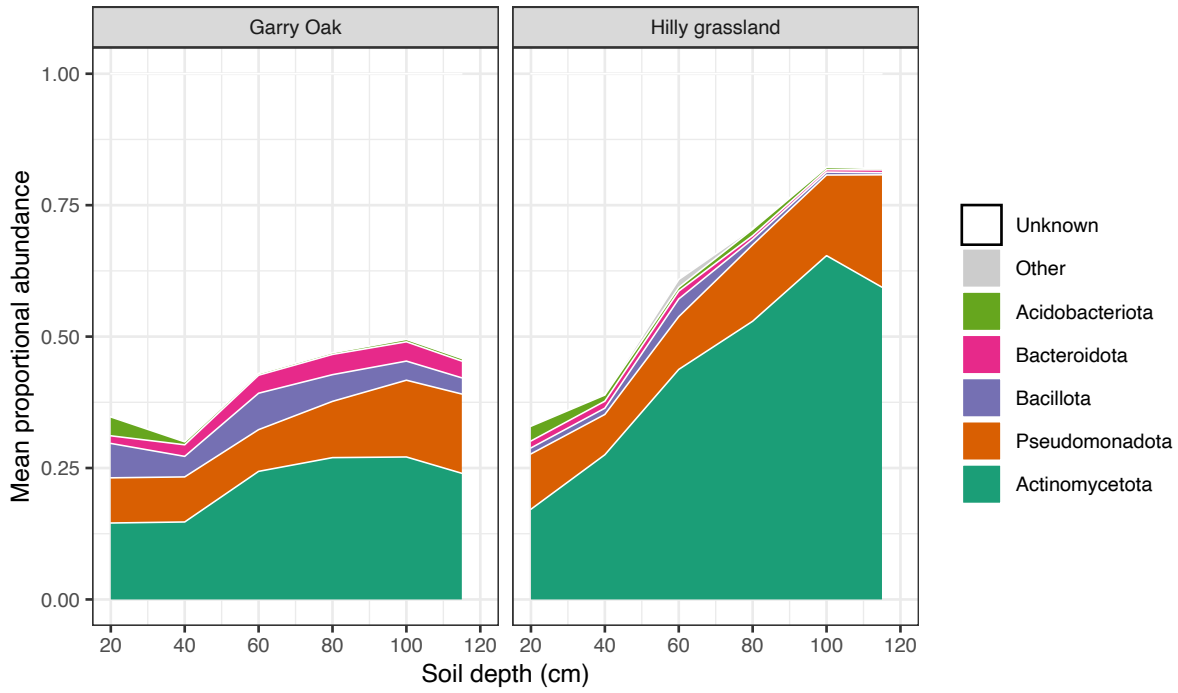

1141

Fig. S13: Relative abundance of hosts of viruses carrying auxiliary metabolic genes. Proportional abundance of vOTUs carrying AMGs plotted across soil depth. Fill colour indicates host phyla.

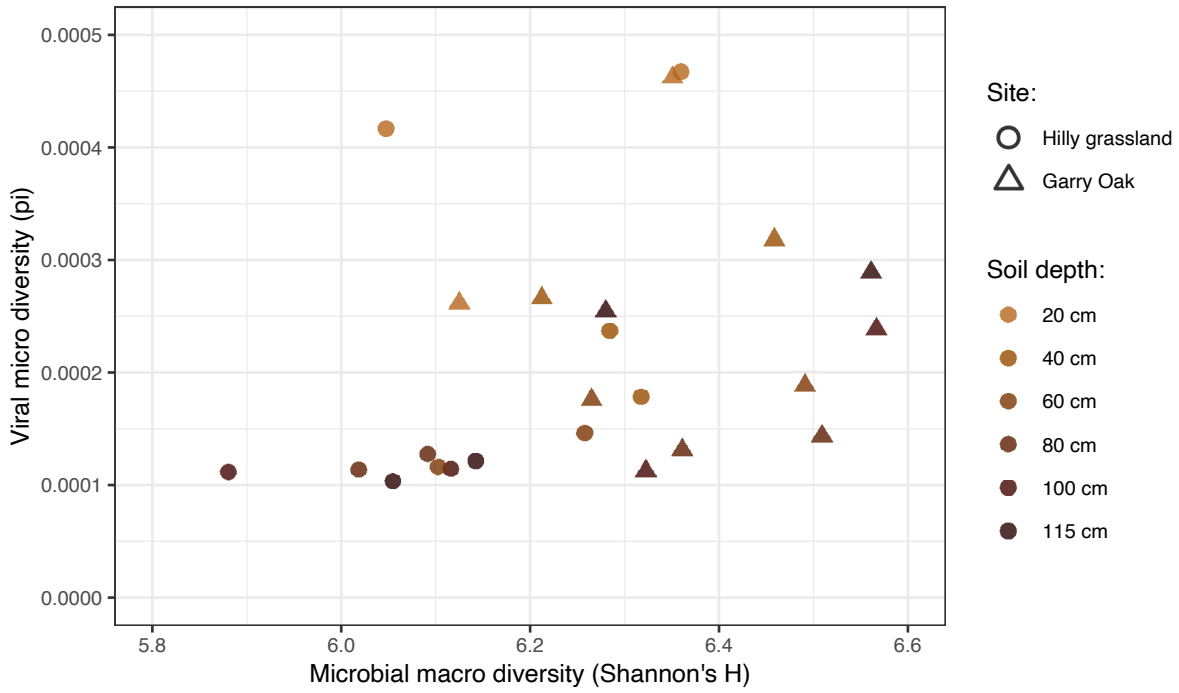

1147

1148 **Fig. S14: Correlation of microbial macro diversity and viral micro diversity.** Shapes
1149 indicate site: Hilly grassland (squares) and Garry Oak (triangles). Shapes are coloured based
1150 on soil depth.
1151